Chapter 3

Sound modeling: source-based approaches

Federico Avanzini

3.1 Introduction: sounds, sources

It was 1971 when Hiller and Ruiz envisioned the possibility of using numerical simulations of the wave equation for sound synthesis applications.

> [...] This is a completely new approach to electronic sound synthesis insofar as the starting point is the physical description of the vibrating object [...]

A decade later McIntyre, Schumacher, and Woodhouse published their classic study on the use of non-linear maps for modeling the generation of self-sustained oscillations in musical instruments.

> [...] a fast minicomputer could produce results at a cycle rate in the audible range. The result would perhaps have some novelty: an electronic musical instrument based on a mathematical model of an acoustic instrument [...]

Today the algorithms described by these authors can be easily implemented in real-time on general-purpose hardware, and it is common practice to use the term *physical modeling* to refer to sound modeling techniques in which the synthesis algorithms are designed based on a description of the physical phenomena involved in sound generation.

Direct sound representations, that are merely based on a description of the sound waveform, do not contain information about the way the sound has been generated and processed by the surrounding environment before arriving to the listener's ear. Sampling in time the sound signal does not assume any underlying structure, or process, or generative model, in sound representation. The symbolic description is extremely poor, and as a consequence very little interaction with the sound representations is allowed. Although signal processing techniques can provide meaningful modifications (e.g. pitch shift, time stretching), sampling is basically a *static*, low-level description of sound.

High level representations of sound signals are necessarily associated with some abstract paradigms that underlie sound production. As we have seen previously, when trying to develop a taxonomy of sound synthesis methods a first distinction can be traced between *signal models* and *source models*. Any algorithm which is based on a description of the sound pressure signal and makes no assumptions on the generation mechanisms belongs to the class of signal models. Additive synthesis is a good example of a signal model: as already mentioned, one major drawback of this technique is its enormous number of control parameters: at least one amplitude and one pitch envelopes have to be specified for each partial. Moreover, the sound representation has not a strong *semantic* interpretation, since these parameters do not have a high-level meaning. Subtractive synthesis with its source-filter structure provides in a sense a more semantic description of sound: in certain cases the two blocks can be given a physical interpretation in terms of an exciting action and a resonating object, respectively. As an example, in the case of LPC based speech synthesis the broadband input signal can be interpreted as a glottal source signal, and the shaping filter represents the action of the vocal tract. However, in many other cases this interpretation does not hold, and the control parameters in the model (e.g., the filter coefficients) do not have a high-level meaning.

Source models aim at describing the physical objects and interactions that have generated an acoustic event rather than the acoustic signal itself. This modeling approach often gives rise to rather complex descriptions, that can lead to computationally expensive numerical algorithms. Several modeling paradigms and techniques are available in the literature for deriving efficient implementations of such descriptions, including lumped/distributed modeling, waveguide structures, finite difference methods, and so on. The following sections describe in detail a few of these approaches. Here it is worth discussing another aspect, i.e. that of control. A direct consequence of assuming a source-based approach is that the resulting control parameters have a straightforward physical interpretation: typical parameters in the models are associated with masses, hardness/softness characteristics, blowing pressures, lengths: such a semantic representation can in principle allow more intuitive interaction.

3.2 Structures, functions, models

3.2.1 Functional blocks

3.2.1.1 Excitations and resonators

Musical oscillators are often strongly non-linear. A typical example is found in woodwind and brass instruments, where self-sustained oscillations in an acoustical bore can only be explained in terms of a non-linear, persistent excitation mechanism. More precisely, the valve (a single or double-reed, or the player's lips) at the bore termination acts as a non-linear element that injects energy into the system. A very similar description holds for bowed string instruments, where the bow is the exciting element. In other cases the instrument is non-linearly excited only for a limited amount of time: a struck string or bar interacts with the hammer or mallet through a non-linear contact force. Values for the contact time are typically a few milliseconds, and after this short excitation the system evolution is linear. There are also examples where non-linearities are negligible: plucked string instruments can be conveniently treated as linear systems (strings and instrument body), where the "pluck" is simply described as a non-equilibrium initial condition (i.e., the pluck gives a string a non-zero displacement distribution and a null velocity distribution).

In all of these cases, the musical instrument can be schematized by means of two main functional blocks, as depicted in Fig. 3.1. The *resonator* is the part of the instrument where the oscillations actually take place. Depending on the instrument, this can be the acoustical bore, the string, the bar.

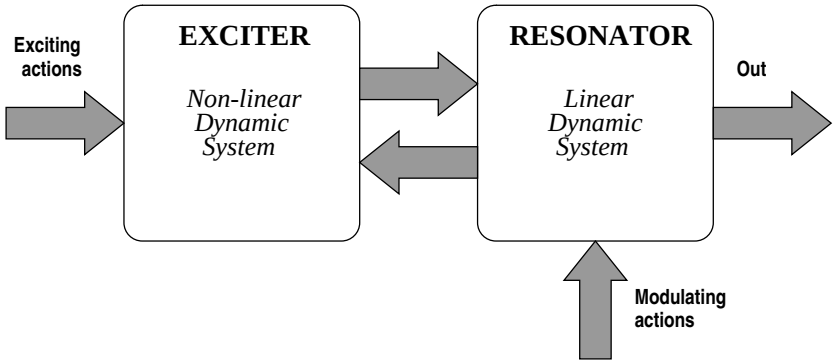

Figure 3.1: Exciter-resonator interaction scheme for a musical instrument (compare to Fig. 3.2(b)).

It is therefore related to such sound attributes as pitch and spectral envelope, and in general to *sound quality*. The *exciter* controls the way energy is injected into the system, thus initiating and possibly sustaining the oscillations. It relates to properties of the transient attack, which is known to have a primary role in defining timbre and *sound identity*.

The interaction between blocks can be feedforward or feedback, depending on the instrument. Persistently excited instruments –such as winds– are described by a feedback structure, while for plucked string instruments a feedforward scheme can be assumed without significant loss in accuracy of the description. A very simple yet striking demonstration of the effectiveness of the exciter/resonator schematization is provided by mounting a clarinet mouthpiece on a flute.[1] The bore boundary conditions are changed from open-open to closed-open so that it plays one octave lower, and the resulting instrument is perceived as a bad sounding clarinet. In other words, the excitation mechanism defines sound identity ("it's a clarinet"), the resonator merely controls sound quality ("it's a *bad* clarinet").

Outlining such functional blocks helps the modeling process; each of them can, to a certain extent, be modeled separately and with different representation strategies. Moreover, the block decomposition can be refined, i.e. both the exciter and the resonator can be described by simpler and more elementary constitutive elements. As an example, the resonating block of a wind instrument is made of a bore, a number of tone holes and a radiating bell, and each of these can be described by their own models. Both "white-box" and "black-box" approaches can be taken. The term white-box indicates that the block is modeled by further decompositions in finer physical elements. The black-box approach amounts to describe a given block according to its input-output behavior, without further assumptions on its internal structure. As an example, the radiating bell in a wind instrument is often modeled using a black-box approach: since the bell acts as a filtering element which reflects low frequencies and radiates high frequencies pressure waves, the modeling problem reduces to filter design.

3.2.1.2 Analogies with speech synthesis

The functional blocks outlined so far can be defined even when we look at speech synthesis techniques. Consider Linear Prediction Coefficients (LPC) synthesis: As already discussed before, the assumption underlying this method is that the phonatory system can be schematized as a feedforward source-filter model, as depicted in Fig. 3.2(a). According to such a schematization, the source block

[1] The author has enjoyed a live demonstration with such a "flarinet", performed by Joe Wolfe while giving a seminar in Venice, 2000.

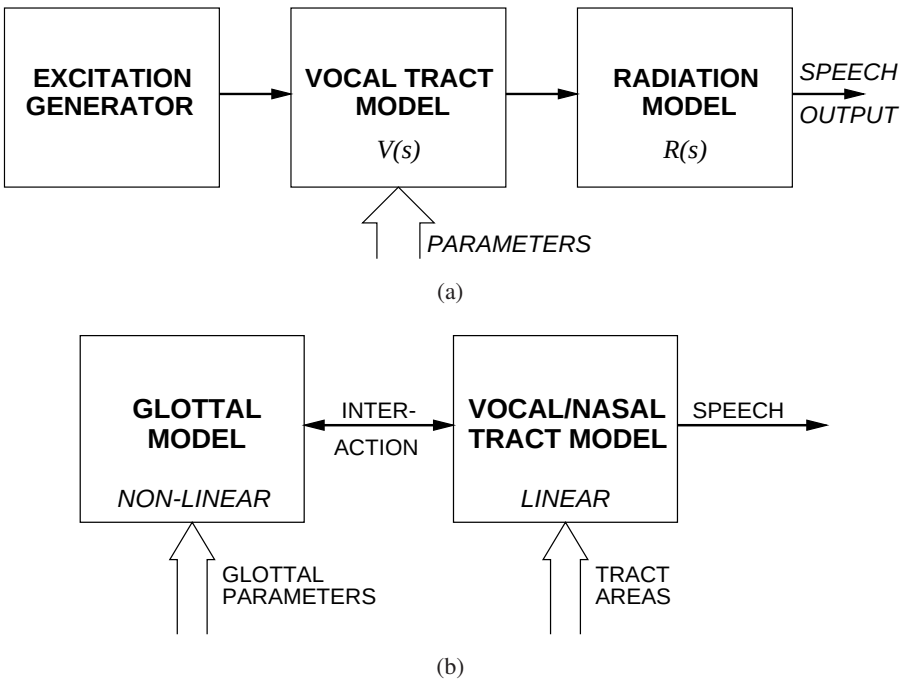

Figure 3.2: Speech synthesizers; (a) feedforward source-filter block scheme associated to LPC based speech synthesis, (b) block scheme of an articulatory speech synthesizer (compare to Fig. 3.1).

represents the airflow at the glottis, while the linear filter accounts for the combined effects of the vocal (and possibly nasal) tract and lip radiation.

Under this interpretation, LPC synthesis is to a certain extent a physically-based technique, since the main blocks depicted in Fig. 3.2(a) can be given a physical and physiological interpretation. However its major assumption, i.e. a feedforward interaction between glottal source and vocal tract, holds only as a first order approximation and is imprecise. In a real phonatory system, the vocal tract behaves as an acoustical air column, thus providing feedback to the vocal source through its input impedance. Detailed modeling has to take into account this acoustical interaction in order to allow for more natural sounding output.

Speech synthesizers that are based on acoustical models are commonly referred to as *articulatory synthesizers*. Figure 3.2(b) depicts a typical block scheme of an articulatory synthesizer. When compared to the scheme in Fig. 3.2(a), it appears to have a very similar structure. However in this case the two main blocks interact in a feedback configuration. On the other hand, this scheme exhibits a striking similarity to the exciter-resonator decomposition outlined above for musical instruments (see Fig. 3.1). The modeling approaches adopted in articulatory speech synthesis are indeed very similar to those used for musical instruments. The vocal tract is a non-uniform, time-varying resonator. As a first approximation, it is described by its cross-sectional area function $A(x,t)$ (x being the position along the tract).

Several approaches are possible for providing excitation signals to an articulatory vocal tract. Parametric models are one option. These fit a given glottal flow waveform using piecewise analytical functions, and are therefore signal models. Alternatively, the vocal tract can be excited by a time varying section that represents the glottis, and driving this additional section using synthesized or measured glottal area signals. However a fully physical description has to account for the interaction

between the glottal source and the resonating vocal tract. Physical models exists that describe the vocal folds by means of one or more masses and viscoelastic elements. Such lumped models can be easily coupled to an articulatory vocal tract and give rise to "natural" interaction effects, that cannot be obtained using simpler feedforward source-filter schemes.

3.2.2 Modeling approaches

As far as modeling paradigms are concerned, these are often grouped into two broad categories, namely *lumped* and *distributed* models. Lumped models are used when a physical system can be conveniently described in terms of ideal masses or rigid bodies, connected to each other with spring and dampers, and possibly non-linear elements. The resulting systems are naturally described in the time domain, in terms of Ordinary Differential Equations (*ODE*s).

Pressure-controlled valves, such as single, double or lip reeds, are typically described using the lumped modeling paradigm. Indeed, these systems are quite complicated: a clarinet reed is a non uniform bar clamped at one termination and free at the other one, and has many vibrational modes. Similarly, a lip reed is made of non-homogeneous tissue and exhibits horizontal and vertical modes of vibration. Nonetheless, these systems have been successfully modeled using lumped elements, and it is widely accepted that such a simplified mechanical description captures the basic behavior of pressure controlled valves. Similar remarks hold for hammers and mallets: during collision, they are deformed and subject to internal losses and non-linear restoring forces. However, interactions with strings and bars have been modeled and efficiently implemented in sound synthesis algorithms by assuming the hammer/mallet to be a lumped mass and deriving empirically the corresponding expression for the contact force.

Distributed models, as opposed to lumped ones, are more often used for describing vibrating bodies or air volumes where forces and matter depend on both time and space. These bodies are not easily decomposed into systems of discrete masses. One-, two- and three-dimensional resonators (such as strings, bars, acoustical bores, membranes, plates, rooms, etc.) are usually treated as distributed systems and mathematically described by means of Partial Differential Equations (*PDE*s). Among the sound synthesis community, however, the most popular approach for dealing with many distributed systems is *waveguide modeling*.

Section 3.3 discusses waveguide models in detail. In its simplest form the method exploits the existence of an analytical solution to the D'Alembert wave equation, which can be seen as a superposition of traveling waves (rigidly translating waveforms). Such a solution can be simulated in the discrete space-temporal domain using delay lines, and the resulting numerical algorithms are extremely efficient and accurate. Moreover, physical phenomena such as frequency dependent losses and dispersion can be included in the models by incorporating low-pass and all-pass filters in the delay line scheme. Again, careful design of such filters allows for very accurate and relatively low-cost simulations. Some sound synthesis algorithms based on the waveguide approach have been successfully implemented on commercial integrated circuit.

Although waveguides are extremely successful in modeling nearly elastic mediums (where the D'Alembert equation or some of its generalizations hold), they are not equally good in dealing with systems where rigidity has a major role and bending forces are the main source of oscillation. As an example, oscillations in a bar are governed by the so called Euler-Bernoulli equation. No analytical general solution is given for this fourth order PDE, and no traveling-waves schematization can be assumed. In order to deal with such systems, *finite difference* or *finite elements* methods are the most suitable techniques. These time-domain techniques are sometimes referred to as "brute force" methods, since they are based on direct discretization of the PDEs and have high computational costs.

On the other hand, when properly used they provide stable and very accurate numerical systems.

Other approaches are available, though less popular, for dealing with distributed systems: cellular models decompose a resonating body into a multitude of interacting particles whose dynamics is discretized and quantized, thus giving rise to a cellular automaton. In the early nineties, Cadoz and his coworkers have introduced CORDIS-ANIMA systems, that describe vibrating bodies as a set of interconnected mass-spring-damper cells. Extremely high computational costs are a major drawback of this approach. Furthermore, no analytical tools are available for assessing stability properties of the discretized systems.

3.3 Distributed models: the waveguide approach

This section introduces the basic concepts of waveguide modeling. Discussion is focused on one-dimensional resonators. No attention is devoted here to higher dimensional waveguide structures.

3.3.1 The origins: the Karplus-Strong algorithm

We start this section on waveguide models with an example which is relevant from many viewpoints. First, the Karplus-Strong (KS hereafter) sound synthesis algorithm is a famous one and deserves to be studied. Second, it contains many of the basic elements that are needed to provide a clear picture of what waveguide modeling is all about, and yet it is structurally simple enough to be discussed in a limited amount of pages. Finally, from a historical perspective it can be regarded as the first prototype of a waveguide approach: it is true that the original formulation of the algorithm did not contain any physical interpretation. What is unquestionable, however, is that the KS algorithm is structurally identical to the simplest waveguide models that we are going to examine in the next sections.

3.3.1.1 The comb filter

The basic computational structure underlying the KS algorithm is the *comb* filter:

$$y[n] = x[n] + R^L y[-L], \quad \Rightarrow \quad H(z) = \frac{1}{1 - R^L z^{-L}} \tag{3.1}$$

The block structure of the filter is given in figure 3.3(a). The poles of $H(z)$ are found from $z^L = R^L$. Therefore the filter has L poles $z = Re^{j2l\pi/L}$ for $l = 0, \ldots L-1$, equally spaced around the circle of radius R. The corresponding frequency response is given is figure 3.3(b). Note that the filter produces a harmonic spectrum in which the frequency peaks are integer multiples of the "fundamental" frequency $f_0 = F_s/L$ Hz.

M-3.1

Find the frequency response of the comb filter (3.1) and plot magnitude and phase responses for various values of R and L.

Figure 3.3(a) already provides us with an intuitive proto-physical interpretation: a perturbation (a wave, as we shall see) propagates through a medium, is confined within a length L, bounces back and forth due to some boundary conditions, has some energy dissipated at each bounce through the coefficient R^L. Note that if the sign of the wave is inverted at each reflection, the resulting filter spectrum is affected:

$$y[n] = x[n] - R^L y[n-L] \quad \Rightarrow \quad H(z) = \frac{1}{1 + R^L z^{-L}} \tag{3.2}$$

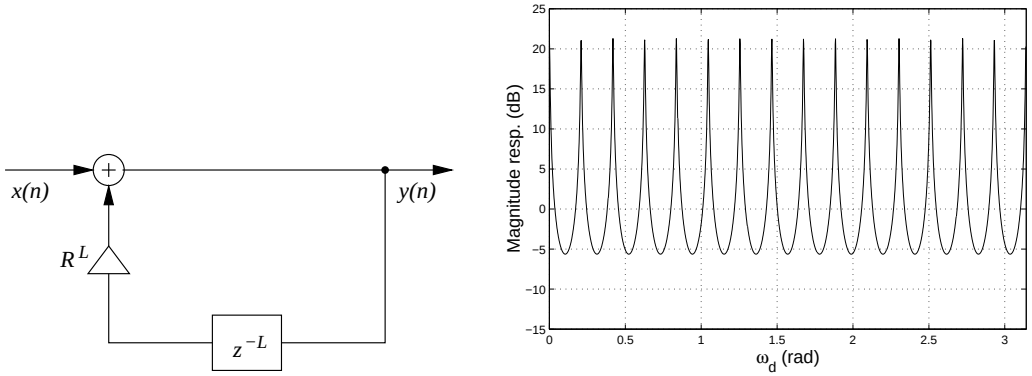

(a) (b)

Figure 3.3: A comb filter; (a) block scheme and (b) frequency response.

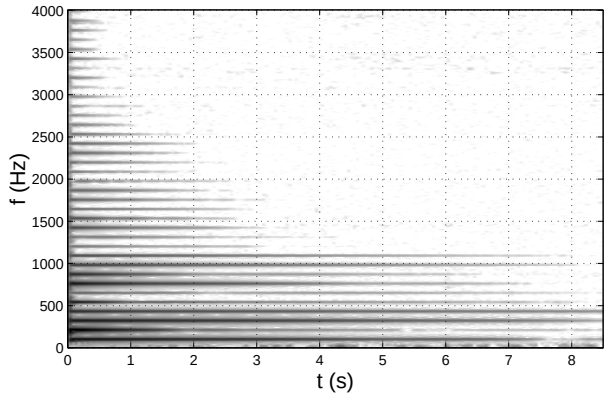

Figure 3.4: . Spectrogram of a plucked A2 guitar string. Note the harmonic structure and the decay rates, which increases with increasing frequency.

In this case the poles are $z = Re^{j(2l+1)\pi/L}$ for $l = 0, \ldots L-1$. This means that the corresponding frequency peaks have all been shifted by an angle π/L with respect to the previous case: now the frequency peaks are *odd* integer multiples of the "fundamental" frequency $f_0 = F_s/(2L)$ Hz. Section 3.3.5 will show that choosing a sign or another corresponds to describing two different boundary conditions (e.g., an open termination versus a closed termination in an acoustical bore).

3.3.1.2 Refining the structure

The above observations suggest that the comb structure (3.1) may be employed to synthesize harmonic sounds, such as those produces by a plucked guitar string. However, in order to obtain something convincing we still have to add some refinements to the structure. Specifically, what it is missing is a mean to control the spectral tilt of the response and to account for different decay rates for the sound partials. Figure 3.4 shows the spectrogram of a guitar sound, from which a frequency-dependent decay pattern can be clearly observed.

In order to account for such a frequency-dependent decay, one can insert a low-pass filter H_{lp} into

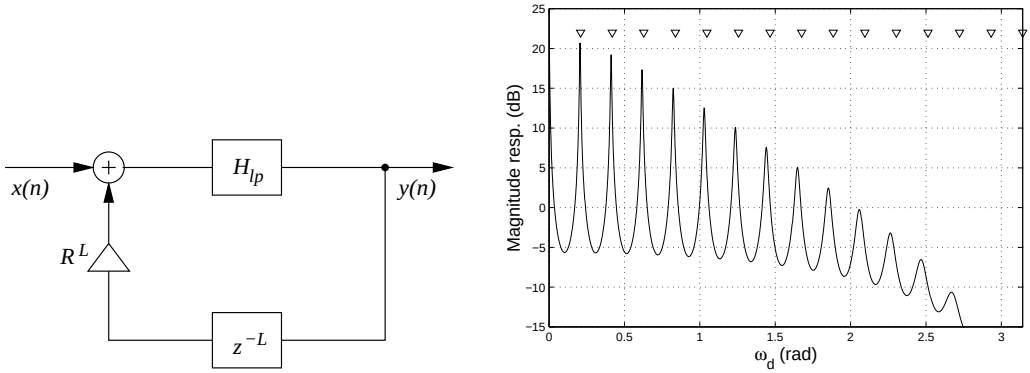

(a) (b)

Figure 3.5: Low-pass comb filter obtained through insertion of a low-pass element into the comb structure; (a) block scheme and (b) frequency response (the triangles mark the harmonic series $l\pi/L,\ l \in \mathbb{N}$).

the feedback loop, as shown in figure 3.5(a): we call this structure a *low-pass comb* filter. Intuitively, at each passage the high-frequency component are attenuated more strongly than low-frequencies component. The simplest low-pass filter that can be employed is a 1^{st} order FIR:

$$y[n] = \frac{1}{2}\left[x[n] + x[n-1]\right] \quad \Rightarrow \quad H_{lp}(z) = \frac{1}{2}\left[1 + z^{-1}\right]. \tag{3.3}$$

The corresponding frequency response is $H_{lp}(f) = \cos(\pi f)e^{-j\pi f}$, from which two remarks can be made: first, the low-pass characteristics of this filter is easily recognized by noting that $|H_{lp}(f)| = \cos(\pi f)$. Second, the filter phase shows that H_{lp} introduces an additional half-sample delay in the loop. As a consequence, the fundamental frequency generated by this structure is now $f_0 = F_s/(L + 1/2)$ Hz. Moreover, a closer analysis would also show that the upper partials are not anymore integer multiples of $f_0 = F_s/(L+1/2)$, due to the insertion of H_{lp} in the loop. These deviations are however very small, especially for the lower partials and for values of R that are close to 1. Figure 3.5(a) shows the frequency response of the comb structure after the insertion of H_{lp}: the (small) deviations from the harmonic series can also be noticed from this plot.

M-3.2

Find the frequency response of the low-pass filter (3.3). Then find the response of the complete system given in figure 3.5 and plot magnitude and phase responses for various values of R and L.

The structure depicted so far is the core of the KS algorithm. On final remark concerns the initial conditions (filter state) to be imposed in order to obtain satisfactory sound output. The choice originally suggested by Karplus and Strong is that of a random initial excitation: although this choice has hardly any physical interpretation,[2] it has the benefit of providing significant initial excitation in the high-frequency region, with a consequent perceptual effect of an initial noisy transient followed by a harmonic steady-state signal.

[2]It would be like imposing initial random displacements to points of a string, as we shall see in the next sections.

M-3.3

Implement the KS algorithm: using the structure given in figure 3.5 and the filter found in M-3.2, write an audio cycle in which the filter is initialized with random excitation and evolves freely. Plot the signal and its spectrogram.

3.3.2 One-dimensional wave propagation

In order to provide a physical interpretation to the KS algorithm, and to fully understand the waveguide approach, we need to review some fundamentals of sound wave propagation in an ideal *elastic* medium. Vibrational phenomena in such a medium are described by the D'Alembert equation, whose one-dimensional version is written as

$$\frac{\partial^2 y}{\partial x^2}(x,t) = \frac{1}{c^2}\frac{\partial^2 y}{\partial t^2}(x,t). \tag{3.4}$$

This equation holds, for instance, in an ideal string of length L, linear mass density μ and tension T. In this case the variable $x \in [0, L]$ stands for position along string length and y stands for *transversal* displacement of the string. The constant c has the value $\sqrt{T/\mu}$ and has the dimensions m/s of a velocity. A full derivation of Eq. (3.4) for the ideal string can be found in many textbooks: roughly speaking, the two main assumptions are that (i) the infinitesimal string segment dx moves only in the vertical direction, so that its acceleration can be computed using only the transverse component of the tension as the acting force; and (ii) the amplitude of the vibrations is very small.

3.3.2.1 Traveling wave solution

A fundamental property of Eq. (3.4) is that it describes *propagation* phenomena. This statement can by proved by factoring the equation as follows:

$$\left(\frac{\partial}{\partial x} - \frac{1}{c}\frac{\partial}{\partial t}\right)\left(\frac{\partial}{\partial x} + \frac{1}{c}\frac{\partial}{\partial t}\right) y = 0. \tag{3.5}$$

From this factorization it is easily seen that generic solutions take the form

$$y(x,t) = y^+(ct - x) + y^-(ct + x). \tag{3.6}$$

The two functions $y^\pm$ describe waveforms that translate rigidly with velocity c, in the right-going and left-going directions, respectively. Their shape is determined by the boundary conditions (in space) and the initial conditions (in time).

Another general solution to equation (3.4) is found by noting that the complex sinusoids $e^{j(\omega t \pm kx)}$, with $k = \omega/c$, are particular solutions of the D'Alembert equation. Depending on boundary conditions, only certain values are allowed for k (and thus for $\omega = kc$). For *fixed* boundaries (i.e. $y(0,t) = y(L,t) = 0$) these turn out to be $k_l = l\pi/L$ with $l \in \mathbb{N}$, i.e. the only allowed frequencies form a harmonic series. Then the Fourier theorem tells us that the general solution is a linear combination of these sinusoids.

A n-dimensional generalization of Eq. (3.4) is found to be

$$\nabla^2 y(\boldsymbol{x},t) = \frac{1}{c^2}\frac{\partial^2 y}{\partial t^2}(\boldsymbol{x},t), \tag{3.7}$$

where the symbol $\nabla^2 = \frac{\partial^2}{\partial x_1^2} + \frac{\partial^2}{\partial x_2^2} + \ldots + \frac{\partial^2}{\partial x_n^2}$ stands for the n-dimensional Laplacian operator. With $n = 2$, Eq. (3.7) describes for instance mechanical vibrations in an ideal membrane, while $n = 3$

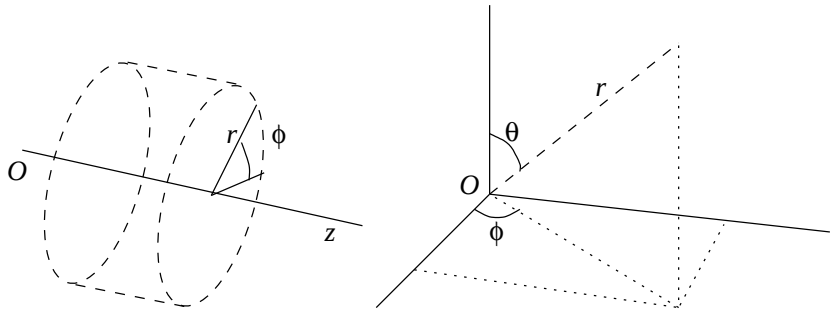

Figure 3.6: Illustration of cylindrical and spherical coordinates.

is well suited for describing acoustic disturbances in an air volume. In this latter case $\boldsymbol{x}$ represents Euclidean coordinates in space and y stands for the acoustic pressure p. As opposed to mechanical vibrations in a string or membrane, acoustic vibrations are *longitudinal* rather than transversal, i.e. the air particles are displaced in the same direction of the wave propagation. Again, simplifying assumptions have been made for deriving Eq. (3.7) in the acoustic case. Namely, disturbances are considered to be small so that the acoustic pressure p is related to density ρ via a linear relation: $p = B(\rho - \rho_{air})/\rho_{air}$, where B is the linearized adiabatic bulk modulus and ρ_{air} is the air equilibrium density. The constant c is then given the value $\sqrt{B/\rho_{air}}$, and again has the dimensions m/s of a velocity.

3.3.2.2 One-dimensional propagation

There are interesting cases where acoustic disturbances can be assumed to be one-dimensional up to a reasonable approximation. Propagation in a cylindrical tube of radius r_0 is an example: by exploiting boundary conditions and symmetries, and looking for harmonic solutions (those with time dependence $\exp(j\omega t)$), the acoustic pressure can be written in cylindrical coordinates as $p(r, \phi, z, t) = \exp(j\omega t) \cdot R(r)Z(z)$ and the equation is separable (see Fig. 3.6 for an illustration of cylindrical coordinates). This leads to the coupled spatial solutions

$$R(r) = \mathcal{I}_0(\beta r), \qquad Z(z) = e^{\pm j\left(k^2 - \beta^2\right)^{1/2} z}, \tag{3.8}$$

where $\mathcal{I}_0$ is the Bessel function of the first kind and zero order. The boundary condition on the cylindrical surface is $d/dr[\mathcal{I}_0(\beta r_0)] = 0$, or equivalently $\mathcal{I}_1(\beta r_0) = 0$. Therefore, only the β values for which $\mathcal{I}_1(\beta r_0) = 0$ are allowed. The first allowed value is obviously $\beta = 0$: this corresponds to the zero-th order modes with $Z(z) = \exp(\pm jkz)$ and $R(r) \equiv 0$, i.e. plane wave propagation along z. The next allowed value corresponds to the first zero of $\mathcal{I}_1$, i.e. $\beta r_0 = 3.83171$. If $r_0 = 8 \cdot 10^{-3}$ m (the approximate radius of a clarinet bore), then $\beta = 479$ m^{-1} and the first corresponding mode in the z direction has a cutoff frequency $f_c = \beta c/2\pi = 26.15$ kHz. Only frequencies higher than f_c do propagate, and they are well out of the range of human hearing. Therefore, for audio applications higher order non-planar modes can be neglected and one-dimensional wave propagation in the z direction can be conveniently described using Eq. (3.4).

Conical geometries are a second example where one-dimensional propagation can be approximately assumed. Again, by exploiting boundary conditions and symmetries and looking for harmonic solutions, pressure can be written in spherical coordinates as $p(r, \theta, t) = \exp(j\omega t) \cdot \Theta(\theta)R(r)$ and the equation is separable (see Fig. 3.6 for an illustration of spherical coordinates). Without going

into details, analysis analogous to that outlined for cylindrical geometries shows that higher-order modes can also be neglected in this case, and propagation in the r direction is conveniently described with zero-th order modes. Since the Laplacian operator is expressed in spherical coordinates as $\nabla^2 = \frac{1}{r^2}\frac{\partial}{\partial r}\left(r^2\frac{\partial}{\partial r}\right) + \frac{1}{r^2\sin\theta}\frac{\partial}{\partial\theta}\left(\sin\theta\frac{\partial}{\partial\theta}\right) + \frac{1}{r^2\sin^2\theta}\frac{\partial^2}{\partial\phi^2}$, the one-dimensional equation for spherical wave propagation is

$$\frac{1}{r^2}\frac{\partial}{\partial r}\left(r^2\frac{\partial R}{\partial r}\right)(r,t) = \frac{1}{c^2}\frac{\partial^2 R}{\partial t^2}(r,t). \tag{3.9}$$

Using the substitution $R = \tilde{R}/r$, it is easily seen that Eq. (3.9) reduces to the one dimensional D'Alembert equation (3.4). Therefore $\tilde{R}$ is the sum of two traveling waves $\tilde{R}^{\pm}$, and the general solution for the zero-th order radial modes is

$$R(r,t) = \frac{1}{r}[\tilde{R}^{+}(ct-r) + \tilde{R}^{-}(ct+r)]. \tag{3.10}$$

3.3.2.3 Wave variables

So far, only displacement y and acoustic pressure p have been considered in the wave equation. However, alternative wave variables can be used in strings and acoustical bores. As an example, the force acting on a string section dx is defined as

$$f(x,t) = -T\frac{\partial y}{\partial x}(x,t) = -T\left[\frac{\partial y^{+}}{\partial x}(ct-x) + \frac{\partial y^{-}}{\partial x}(ct+x)\right] = \frac{T}{c}\dot{y}^{+}(ct-x) - \frac{T}{c}\dot{y}^{-}(ct+x).$$

Therefore, using this equation force waves $f^{\pm}$ can be defined as $f^{\pm} := \mp\frac{T}{c}\dot{y}^{\pm}$. On the other hand, the transversal velocity wave variable in the same string is given by

$$v(x,t) = \frac{\partial y}{\partial t}(x,t) = \dot{y}^{+}(ct-x) + \dot{y}^{-}(ct+x).$$

From this, velocity waves $v^{\pm}$ are defined as $v^{\pm} := \dot{y}^{\pm}$. The pair of force and velocity variables is sometimes referred to as *Kirchhoff variables*, in analogy with voltage and current in electrical systems (Sec. 3.4 provides a detailed discussion of Kirchhoff variables and analogies between electrical, mechanical and acoustic systems). From the previous equations it immediately follows that

$$f^{\pm}(ct \mp x) = \pm Z_0 v^{\pm}(ct \mp x), \qquad \text{with} \qquad Z_0 = T/c = \sqrt{T\mu}. \tag{3.11}$$

The quantity Z_0 takes the name of *wave* (or *characteristic*) *impedance* of the string, and its reciprocal $\Gamma_0 = Z_0^{-1}$ is termed *wave admittance*. Note that using Z_0 both the force f and the velocity v can be related to the force waves $f^{\pm}$. Namely, the following relations hold:

$$\begin{aligned} f &= f^{+} + f^{-}, & v &= \frac{1}{Z_0}\left[f^{+} - f^{-}\right], \\ f^{+} &= \frac{f + Z_0 v}{2}, & f^{-} &= \frac{f - Z_0 v}{2}, \end{aligned} \tag{3.12}$$

that transform the pair (f, v) into the pair (f^{+}, f^{-}), and vice versa. Wave impedance can be defined also in a cylindrical bore. In this case the Kirchhoff variables are taken to be pressure p and flow u (volume velocity). These can be related through the wave impedance Z_0: $p^{\pm}(ct \pm x) = \pm Z_0 u^{\pm}(ct \pm x)$, where $Z_0 = \rho_{air}c/S$ and S is the constant cross-sectional area of the bore. For conical geometries, the cross-section S is not constant and the definition of Z_0 has to be generalized. The wave impedance

is then defined as a function $Z_0(s)$ such that the relations $P^{\pm}(r,s) = \pm Z_0(s)U^{\pm}(r,s)$ hold in the Laplace domain. It can be seen that $Z_0(s) = \rho_{air}c/S \cdot [rs/(rs+c)]$.

Summarizing, this section has shown that vibrational phenomena in many elastic media can be described as one-dimensional wave propagations. Furthermore, Kirchhoff and wave variables in these media are related through wave impedance. This results provide the basis for developing 1-D waveguide structures.

3.3.3 Basic waveguide structures

3.3.3.1 Delay lines

Waveguide models exploit the existence of the solution (3.6) to the D'Alembert equation and discretize this solution instead of the differential equation itself. This remark explains to a large extent why waveguide structures are much more efficient than finite difference methods in simulating vibrations of elastic media, at least in the 1-D case.

Consider a pressure distribution $p = p^+ + p^-$ inside an ideal lossless cylindrical bore. If T_s is the sampling period, a suitable choice for the spatial sampling step is $X_s = cT_s$. Thus, a discretized version of p is obtained through the variable substitution $x \mapsto mX_s$ and $t \mapsto nT_s$ (with $m, n \in \mathbb{N}$), and leads to

$$p[mX_s, nT_s] = p^+[ncT_s - mX_s] + p^-[ncT_s + mX_s] = p^+[(n-m)cT_s] + p^-[(n+m)cT_s].$$

Removing the constant sampling steps yields:

$$p[m,n] = p^+[n-m] + p^-[n+m]. \tag{3.13}$$

The term $p^+[n-m]]$ in Eq. (3.13) can be thought of as the output from a digital delay line of length m, whose input is $p^+[n]$. Analogously, the term $p^-[n+m]$ can be thought of as the input of a digital delay line with the same lenght, whose output is $p^-[n]$. This remark leads to the definition of a *waveguide section* as a bidirectional delay line, as depicted in Fig. 3.7(a). Note that the horizontal direction of this structure has a straightforward physical interpretation: it corresponds to the position x along the axis of the cylindrical bore. In the example depicted in Fig. 3.7, two "observation points" have been chosen at $x = 0$ and $x = mX_s = L$. At these points, the pressure signal at time n is reconstructed by summing the corresponding pressure waves $p^{\pm}$. A very similar structure can be outlined for numerically simulating a pressure distribution in an ideal lossless conical bore. In this case, propagation is described by the one-dimensional equation (3.9), whose general solution is given by Eq. (3.10). The conical waveguide is therefore defined as in Fig. 3.7(b). Observation points can be chosen analogously to the cylindrical case.

3.3.3.2 Boundary conditions

Looking at figure 3.7 we immediately realize that we still need a final step in order to come out with a computational structure that describes e.g. a string with fixed ends or a cylindrical section with open ends: boundary conditions. Ideal conditions can be immediately derived by observing equation (3.12). Take as an example a string of length L with fixed end: these boundary conditions mean that $v(0) = v(L) = 0$, from which the reflection rules $f^+(0) = f^-(0)$ and $f^-(L) = f^+(L)$ are derived.[3]

[3]Now go back to figure 3.3(b): the comb filter can be viewed as a pair of waveguide sections of length $L/2$ samples, with reflection rules that correspond to fixed end conditions.

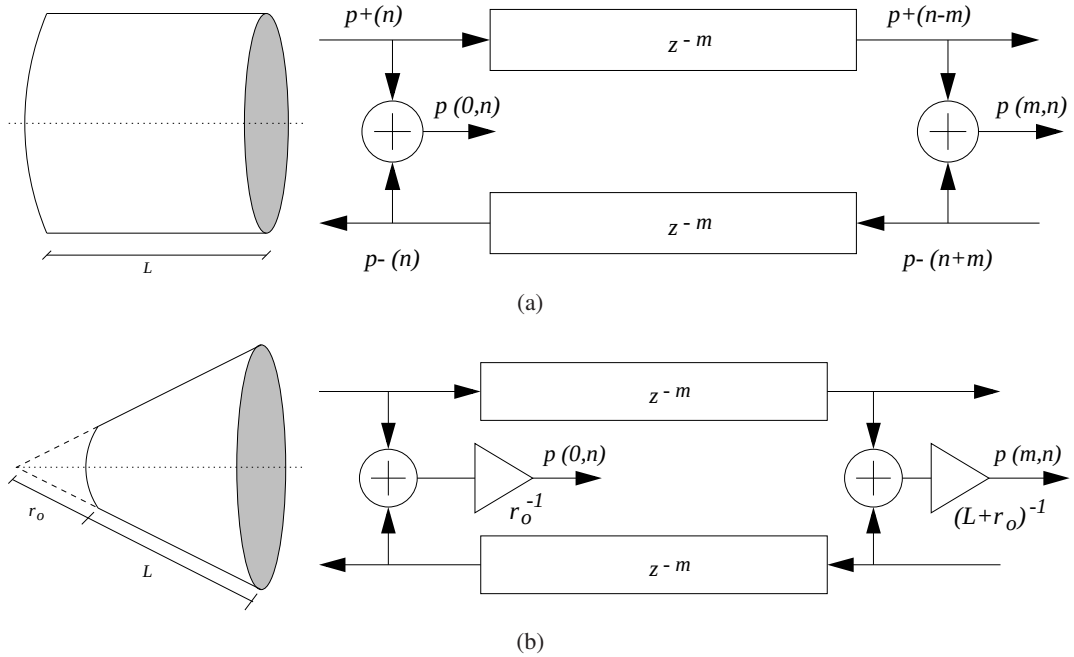

Figure 3.7: Lossless waveguide sections with observation points at position $x = 0$ and $x = mX_s = L$; (a) cylindrical section; (b) conical section.

Analogously, take a cylindrical bore of length L, with a closed end at $x = 0$ and an open end at $x = L$: the first condition implies $u(0) = [p^+(0) - p^-(0)]/Z_0 = 0$ (no flow through a closed end), which in turn implies the reflection condition $p^+(0) = p^-(0)$; the second one implies $p(L) = p^+(L)+p^-(L) = 0$ (p matches the atmospheric pressure at the open boundary), which in turn implies the reflection condition $p^-(L) = -p^+(L)$.

M-3.4

Write the WG filter of a string of length L (in meters), using a sample rate $F_s = 44.1$ kHz. Assume the string is fixed at both ends.

3.3.4 Modeling real world phenomena

As already mentioned, the waveguide structures introduced above describe *ideal* systems, i.e. ideally elastic media, where the D'Alembert equation (3.4) or its spherical version (3.9) hold. Real systems exhibit more complex behaviors.

3.3.4.1 Dissipation

Energy *dissipation* occurs in any real vibrating medium. In an acoustical bore this is due to air viscosity, thermal conduction and wall losses. Dissipation in a string comes from internal losses related to elastic properties of the material, energy transfer through terminations, and friction with air. For clarity, consider the pressure distribution in a cylindrical bore. In the simplest approximation, all of the dissipation phenomena can be incorporated in the D'Alembert equation by including an

additional term proportional to the first time derivative:

$$\frac{\partial^2 p}{\partial t^2}(x,t) = c^2 \frac{\partial^2 p}{\partial x^2}(x,t) - \epsilon \frac{\partial p}{\partial t}(x,t). \tag{3.14}$$

In the limit of small ϵ, Eq. (3.14) still admits a traveling wave solution, which can be digitized with the same procedure described in the ideal case:

$$\begin{aligned} &p(x,t) = e^{-\frac{\epsilon x}{2c}} p^+(ct-x) + e^{\frac{\epsilon x}{2c}} p^-(ct+x), && \text{then} \\ &p[m,n] = g^m p^+[n-m] + g^{-m} p^-[n+m], && \text{with} \quad g = e^{-\frac{\epsilon T_s}{2}} < 1. \end{aligned} \tag{3.15}$$

Thus the traveling waves are exponentially damped along the propagation direction, and this phenomenon can be easily incorporated in the waveguide structure. This is shown in Fig. 3.8(a), where losses have been consolidated, or *lumped*, in a single multiplier cascaded to the delay line. The loss factor g^m summarizes the distributed losses occurring in the spatial interval $[0, mX_s]$. In most of real phenomena, however, losses increase with frequency. A better approximation of dissipation phenomena can account for this frequency dependence by substituting the constant factor g with a lowpass filter $G(z)$. Moreover, in order to avoid frequency dependent delay, $G(z)$ must be a zero-phase FIR filter. Alternatively, a linear-phase filter can be used; in this case the length of the delay line has to be reduced correspondingly, in order to obtain the desired overall delay.[4]

M-3.5

Add loss factors g and a low-pass dissipation filter to the WG filter of a string developed in M-3.4 (use e.g. the low-pass FIR (3.3)). Study the frequency response of this system.

3.3.4.2 Dispersion

A second important phenomenon in natural wave propagation is that of *dispersion*. In a string, dispersion is introduced by string stiffness. This is usually modeled in the D'Alembert equation (3.4) by introducing an additional term proportional to the fourth spatial derivative:

$$\frac{1}{c^2}\frac{\partial^2 p}{\partial t^2}(x,t) = \frac{\partial^2 p}{\partial x^2}(x,t) - \epsilon \frac{\partial^4 p}{\partial^4 x}(x,t), \tag{3.16}$$

where the dispersive correction term ϵ is proportional to the string Young's modulus. If ϵ is small, its first order effect is to increase the wave propagation speed with frequency:

$$c(\omega) = c_0 \left(1 + \frac{\epsilon \omega^2}{2c_0^2}\right), \tag{3.17}$$

where c_0 is now the wave travel velocity in the absence of dispersion. Equation (3.17) states that a traveling wave is no longer a rigid shape that translate at constant speed. Instead, frequencies "disperse" as they propagate with different velocities. As a consequence, the frequencies f_k of the allowed partials are not harmonic, instead they are stretched onto an inharmonic series according to the equation

$$f_k = k f_0 I_k, \quad \text{where} \quad I_k \approx \sqrt{1 + Bk^2},$$

[4] Now go back to figures 3.3(b) and 3.5(b): the parameter R^L plays the role of the loss factor g^m, while the linear-phase FIR filter H_{lp} plays the role of $G(z)$ and introduces frequency-dependent dissipation.

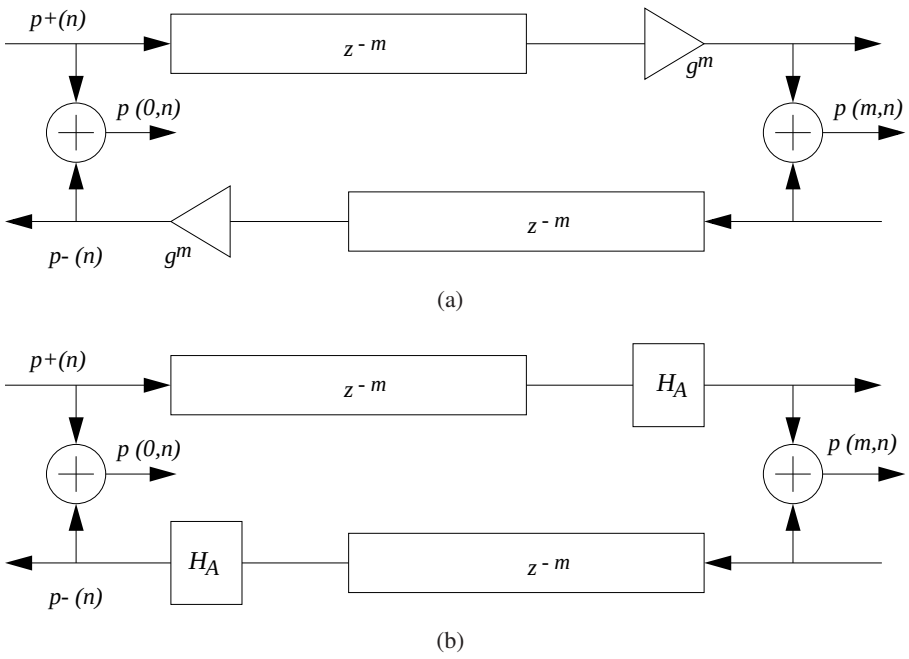

Figure 3.8: Waveguide simulation of non-ideal media; (a) frequency independent dissipation; (b) dispersion.

and where $B = \pi^2\epsilon/L^2$. The quantity I_k is usually termed *index of inharmonicity*. Dispersion is particularly important in piano strings, where the lower tones exhibit significant inharmonicity.

Having a non-uniform wave velocity $c(\omega)$ implies that it is not possible to define a sampling step as $X_s = c_0 T_s$. Instead, it can be said that a component with frequency $f = \omega/(2\pi)$ travels a distance $c_0 T_s$ in the time interval $c_0 T_s / c(\omega)$. As a consequence, the unitary delay z^{-1} has to be substituted with the all-pass filter $H_a(z) = z^{-c_0/c(\omega)}$, which has a unitary magnitude response but non-constant phase delay. Similarly to dissipative low-pass filters, m all-pass delays can be *lumped* in a single filter H_a^m. Moreover, the linear and non-linear parts of the phase response can be treated separately. H_a^m can thus be written as $H_a^m(z) = z^{-m} \cdot H_A(z)$, where $H_A(z)$ is another all-pass filter approximating the non-linear part of the phase response. In summary, a dispersive resonator is modeled as in Fig. 3.8(b).

3.3.4.3 Length tuning

One last improvement to the basic waveguide structure of Fig. 3.7 is provided by *fractional delay lines*. It is easily verified that with a sampling rate $F_s = 44.1$ kHz and with a wave velocity $c = 347$ m/s (sound velocity in air at 20 C°), the resulting spatial step is $X_s = 7.8 \cdot 10^{-3}$ m. This distance produces perceivable pitch variations in a wind instrument. It is therefore necessary to design fractional delays in order to provide fine tuning of the length of a waveguide section. Without going into details, this can be ideally achieved by including an additional filter in the structure, with flat magnitude response (that does not affect the overall magnitude response of the waveguide structure) and linear phase response (that adds the desired fractional delay). Both interpolation filters (FIR) and all-pass filters (IIR) can be used for approximating such characteristics.

3.3.5 Junctions and networks

The last section has introduced the main concepts of waveguide modeling for a signal propagating in a *uniform* medium. When discontinuities are encountered, the wave impedance changes and signal *scattering* occurs, i.e. a traveling wave is partially reflected and partially transmitted. Examples of non-uniform media are a cylindrical bore where the cross-sectional area changes abruptly, or a string where the value of the linear mass density jumps changes discontinuously. In order to model these discontinuities, appropriate junctions have to be developed, that connect two (or more) waveguide sections. The boundary reflection conditions that we have examined at the end of section 3.3.3 can be regarded as special cases of junctions, as discussed in the following paragraphs.

3.3.5.1 The Kelly-Lochbaum junction

Consider two cylindrical bores, with cross-sectional areas $S_{1,2}$ and wave admittances $\Gamma_{1,2} = Z_{1,2}^{-1} = S_{1,2}/\rho_{air}c$, connected to each other. Analysis of this problem leads to the derivation of the well known *Kelly-Lochbaum* junction. First of all, physical constraints have to be imposed on the Kirchhoff variables p, u at the junction, namely pressures $p_{1,2}$ must have the same value p_J and the flows $u_{1,2}$ from the two sides must sum to zero:

$$u_1 + u_2 = 0, \qquad p_1 = p_2 = p_J. \tag{3.18}$$

Using the Kirchhoff analogy $p \leftrightarrow v$ (voltage) and $u \leftrightarrow i$ (current), Eqs. (3.18) can be regarded as describing a parallel junction. If pressure wave variables are introduced as in Eq. (3.12) (with p^+ and p^- denoting incoming and outgoing waves, respectively), and the junction pressure p_J is used, then the relation $p_l^- = p_J - p_l^+$ (for $l = 1, 2$) holds. Substitution in the first of Eqs. (3.18) yields

$$\begin{aligned} 0 &= (u_1^+ + u_1^-) + (u_2^+ + u_2^-) = \Gamma_1(p_1^+ - p_1^-) + \Gamma_2(p_2^+ - p_2^-) = \\ &= \Gamma_1(2p_1^+ - p_J) + \Gamma_2(2p_2^+ - p_J). \end{aligned}$$

From this, the junction pressure p_J can be expressed in terms of the incoming pressure waves $p_{1,2}^+$ as

$$p_J = 2\frac{\Gamma_1 p_1^+ + \Gamma_2 p_2^+}{\Gamma_1 + \Gamma_2}.$$

Using this latter expression, the outgoing pressure waves $p_{1,2}^-$ can be written as

$$\begin{aligned} p_1^- &= p_J - p_1^+ = -\frac{\Gamma_2 - \Gamma_1}{\Gamma_2 + \Gamma_1}p_1^+ + \frac{2\Gamma_2}{\Gamma_2 + \Gamma_1}p_2^+, \\ p_2^- &= p_J - p_2^+ = \frac{2\Gamma_1}{\Gamma_2 + \Gamma_1}p_1^+ + \frac{\Gamma_2 - \Gamma_1}{\Gamma_2 + \Gamma_1}p_2^+. \end{aligned}$$

If the *reflection coefficient* ρ is defined as

$$\rho := \frac{\Gamma_2 - \Gamma_1}{\Gamma_2 + \Gamma_1},$$

then Eqs. (3.19) become

$$\begin{aligned} p_1^- &= -\rho\, p_1^+ + (1+\rho)p_2^+, \\ p_2^- &= (1-\rho)p_1^+ + \rho\, p_2^+. \end{aligned} \tag{3.19}$$

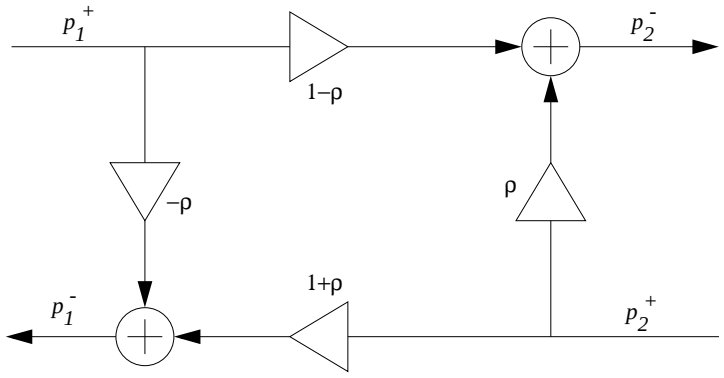

Figure 3.9: Kelly-Lochbaum junction for two cylindrical bores with different areas.

These equations describe the Kelly-Lochbaum junction. A scattering diagram is depicted in Fig. 3.9.

This junction has been extensively used in what are often termed "multitube lossless models" of the vocal tract. These are basically articulatory models where the vocal tract shape is approximated as a series of concatenated cylindrical sections. Pressure wave propagation in each section is then described using digital waveguides, and interconnections are treated as Kelly-Lochbaum junctions. Remarkably, the same junction can be used to describe not only acoustic, but also mechanical structures. As an example, consider two strings with different densities, connected at one point: this can be thought of as a series junction, since the physical constraints impose that velocity (i.e., "current") has to be the same on the left and right sides, and the sum of forces (i.e., "voltages") from the two sides must be zero. Analogously to the above analysis, a series Kelly-Lochbaum junction can be derived in this case.

Terminations of a waveguide model are an interesting particular case of junctions. Consider an ideal cylindrical bore, closed at one end: this boundary condition corresponds to an infinite impedance $Z_2 = \infty$ (i.e., $S_2 = 0$), and thus to a reflection coefficient $\rho = -1$. In other words, complete reflection occurs and the relation $p_1^-(0,t) = p_1^+(0,t)$ holds. Similarly, an ideally open end can be seen to correspond to $Z_2 = 0$ (i.e., $S_2 = \infty$), and thus to $\rho = 1$: this is a second case where complete reflection occurs, namely the relation $p_1^-(0,t) = -p_1^+(0,t)$ holds. These reflection conditions are identical to the ones that we have derived in section 3.3.3 (analogous considerations hold for string terminations).

Figure 3.10 shows an example where different junctions have been used and combined into a waveguide model. Note that in this example the scattering junction between the two cylindrical sections is not in the Kelly-Lochbaum form; instead, a *one-multiply scattering junction* is used, which allows more efficient implementation of Eqs. (3.19). Open- and closed-tube terminations are modeled according to the above remarks.

M-3.6

Realize the structure of figure 3.10. Add loss factors g and a low-pass dissipation filter to each WG section, as done in M-3.5. Study the frequency response of this system.

3.3.5.2 N-dimensional junctions

The result expressed in Eq. (3.19) can be easily extended to higher dimensions. Consider parallel junction of N acoustical bores. In this case a *scattering matrix* can be found, and Eq. (3.19) is

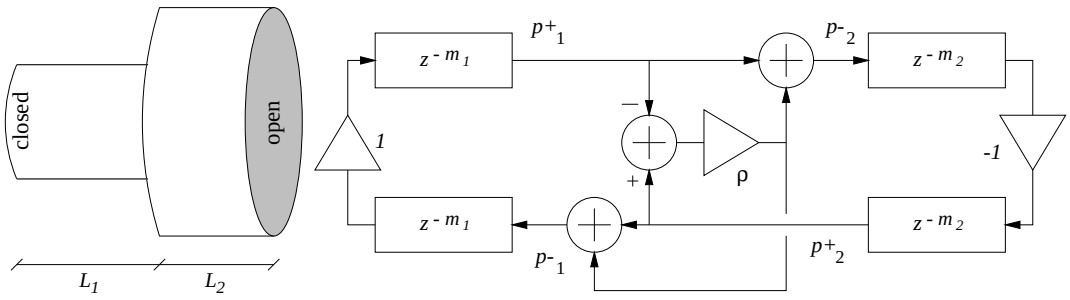

Figure 3.10: Example of an acoustic model implemented with waveguide sections an junctions.

generalized to

$$\boldsymbol{p}^- = \boldsymbol{A} \cdot \boldsymbol{p}^+, \tag{3.20}$$

where $\boldsymbol{p}^\pm$ are n-dimensional vectors whose elements are the incoming and outgoing pressure waves in the n bores. The physical constraints expressed in Eq. (3.18) are also generalized in an obvious way, and calculations analogous to those outlined for the Kelly-Lochbaum junction lead to the result

$$\boldsymbol{A} = \begin{bmatrix} \frac{2\Gamma_1}{\Gamma_J} - 1, & \frac{2\Gamma_2}{\Gamma_J}, & \cdots & \frac{2\Gamma_N}{\Gamma_J} \\ \frac{2\Gamma_1}{\Gamma_J}, & \frac{2\Gamma_2}{\Gamma_J} - 1, & \cdots & \frac{2\Gamma_N}{\Gamma_J} \\ \vdots & & \ddots & \vdots \\ \frac{2\Gamma_1}{\Gamma_J}, & \frac{2\Gamma_2}{\Gamma_J}, & \cdots & \frac{2\Gamma_N}{\Gamma_J} - 1 \end{bmatrix}, \qquad \text{where} \quad \Gamma_J = \sum_{l=1}^{N} \Gamma_l. \tag{3.21}$$

Note that when $N = 2$ Eq. (3.20) reduces to the Kelly-Lochbaum equations.

3.3.5.3 Non-cylindrical geometries

A final remark is concerned with junctions of conical elements. Generalizing the cylindrical case is not straightforward, since the derivation of Kelly-Lochbaum equations is based on the implicit assumption of plane wave propagation. This assumption permits imposition of the constraints (3.18) on a flat scattering boundary, which is a wavefront for both p_1 and p_2. But wavefronts in conical sections are spherical and this circumstance makes it impossible to define a unique surface on which boundary conditions can be applied: Fig. 3.11(a) shows that there is a region between the two spherical wavefronts which is within neither conical segment. This ambiguity in the definition of the scattering boundary is usually overcome by assuming that the transition volume is small and thus pressure is constant inside the volume. Under this assumption, continuity conditions analogous to (3.18) are imposed and the reflection coefficient ρ is generalized to a first order filter $R(s)$.

However, a second and more serious problem arises when one looks at the nature of $R(s)$. This filter turns out to be unstable (non-causal growing exponential) in the case of the convex configuration depicted in Fig. 3.11(b). While this circumstance is physically consistent (in the continuous-time domain the scattered waves can grow exponentially only for a limited time because they are cancelled out by subsequent multiple reflections), in a numerical simulation the system can turn out unstable, due to the approximations introduced by the discretization process and to round-off errors introduced by finite-precision.

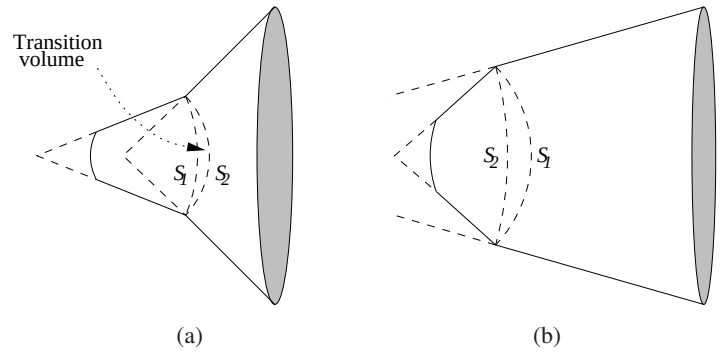

Figure 3.11: Boundary regions for (a) non-convex and (b) convex conical junctions.

3.4 Lumped models

3.4.1 Building blocks and analogies

In a large class of systems it is possible to construct pairs of variables (hereafter defined as *Kirchoff variables*) with the property that their product has the dimensions of power (Kg m^2/s^3). In electrical systems such a pair of variables is given by (v, i), voltage and current. Integro-differential relations can be found that relate these two variables, in particular three elementary relations define the fundamental quantities resistance R, inductance L and capacitance C. In the Laplace domain, the integro-differential equations are turned into simple algebraic relations:

$$V(s) = R \cdot I(s), \qquad V(s) = sL \cdot I(s), \qquad V(s) = \frac{1}{sC} I(s). \tag{3.22}$$

These are particular examples of a more general relation in linear electric circuits:

$$V(s) = Z(s)I(s), \tag{3.23}$$

where the quantity $Z(s)$ is called *impedance* of the circuit and is defined as the ratio between the Laplace transforms of voltage and current intensity. The inverse of $Z(s)$ is called *admittance*, and it is usually denoted as $\Gamma(s) = Z(s)^{-1}$.

3.4.1.1 Mechanical systems

An pair of variables analogous to voltage and current are found in mechanical systems: force f (Kg m/s^2) and velocity v (m/s) satisfy the same condition of voltage and current, i.e. their product is a power. Therefore, f and v are taken as mechanical Kirchhoff variables. Again, the ratio of these two variables in the Laplace domain is defined as (mechanical) *impedance*, and its inverse is the (mechanical) admittance. Using three notable relations between f and v, it is possible to introduce mechanical equivalents of resistance, capacitance and inductance.

The simplest relation is direct proportionality: $f(t) = rv(t)$. This is used to define ideal linear viscous forces, and comparison with the first of Eqs. (3.22) permits r to be regarded as a mechanical resistance. Newton's second law of classical dynamics provides a second relation: the inertial mass m of a non-relativistic body is defined as the ratio between the total force acting on it and its acceleration, i.e. $f(t) = ma(t) = m\dot{v}(t)$. In the Laplace domain this is turned into $F(s) = msV(s)$, and from

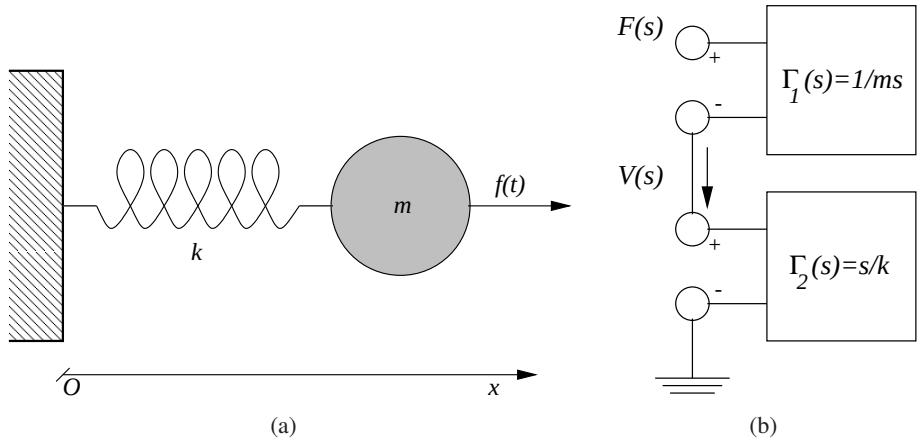

Figure 3.12: A mass pulled by a linear spring; (a) mechanical system and (b) combination of one-ports in series.

comparison with the second equation in (3.22) m is seen to be equivalent to an inductance. Finally, Hooke's law provide an analogy to electrical capacitance: in an ideal linear spring the elastic force is proportional to the elongation of the spring: $f(t) = kx(t) = k\int_0^t v(\tau)d\tau$. Again, in the Laplace domain this is turned into $F(s) = k/s\ V(s)$, and comparison with the third of Eqs. (3.22) shows that the stiffness constant k of the spring corresponds to the reciprocal of a capacitance. Summarizing, the analogies between mechanical and electrical elements are as follows:

$$\begin{array}{ccc} F(s) = r \cdot V(s), & F(s) = \dfrac{k}{s} V(s), & F(s) = ms \cdot V(s), \\ \Downarrow & \Downarrow & \Downarrow \\ r \sim R, & \dfrac{1}{k} \sim C, & m \sim L. \end{array} \tag{3.24}$$

Figure 3.12(a) shows the simplest example of a "series" junction between these mechanical elements: a mass attached to an ideal linear spring and driven by an external force. The system's dynamics are described by the equation

$$m\ddot{x}(t) = -kx(t) + f(t), \qquad \Rightarrow \qquad F(s) = \left(ms + \frac{k}{s}\right) V(s). \tag{3.25}$$

The second equation (3.25) shows that the aggregate impedance $Z(s)$ of the system is the sum of the two elementary impedances $Z_1(s) = ms$ and $Z_2(s) = k/s$.

The above discussion is the starting point for developing one-port network theory for mechanical systems. The one port is defined as a black-box with a single pair of input/output terminals, as in Fig. 3.12(b). A force is applied at the terminals, analogously to an electrical potential, and velocity "flows" as electrical current. Instantaneous power and energy can be defined and used to characterize *passive* and *lossless* one-ports. Connections through ports can be made using Kirchhoff's Laws, so that series and parallel junctions are defined analogously to circuit theory. In circuit theory terminology, the two one-ports in Fig. 3.12(b) share a common velocity, thus they are connected in series.

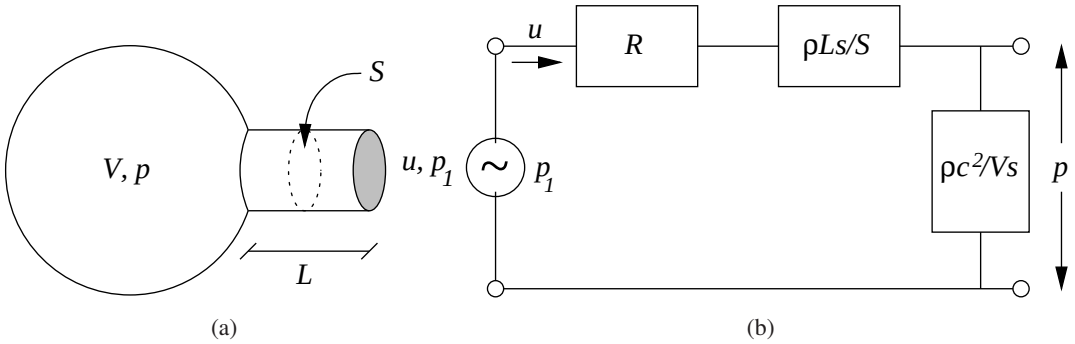

Figure 3.13: A Helmholtz resonator driven by an external acoustic wave; (a) acoustic system and (b) circuit representation.

3.4.1.2 Acoustic systems

Acoustic systems can also be described in terms of lumped elements only, in certain situations. In particular, when the dimensions of an acoustical element are much less than the sound wavelength, then the acoustical pressure, p can be assumed constant. In this case, the acoustic behavior of the element is, at least at low frequencies, very simple. Note that the acoustic pressure p (Kg/ms^2) and the volume velocity u (m^3/s) are such that their product is a power, and can therefore be used as a pair of Kirchhoff variables.

Resistive phenomena are observed during the passage of acoustic airflow through a small opening. In this case the flow behavior is dominated by viscous and thermal losses and it is reasonably assumed to be in phase with the acoustic pressure, therefore the relation $p(t) = Ru(t)$ holds at the opening where the constant R is termed *fluid-dynamic resistance*. Fluid-dynamic inductance is defined in a short, open tube having cross-sectional area S and length L. The air mass inside the bore is then $m = \rho_{air}SL$ (ρ_{air} being the air density). Suppose that an acoustic pressure $p(t)$ is applied to one end of the tube; then the enclosed air behaves like a lumped mass driven by the force Sp, and Newton's law implies

$$Sp(t) = \rho_{air}SL \cdot \dot{v}(t), \qquad \Leftrightarrow \qquad P(s) = \frac{\rho_{air}L}{S} \cdot sU(s),$$

where the relation $u(t) = Sv(t)$ has been used, and $v(t)$ indicates particle velocity. Finally, capacitance is associated with air volumes. Consider the volume $V(t)$ of air inside a cavity; the contraction $dV(t)$ caused by an acoustic pressure $p(t)$ is such that $-\rho_{air}c^2 \cdot dV/V = p$, where $\rho_{air}c^2$ is the bulk modulus of air at atmospheric pressure. As a consequence, a new air volume $-dV$ can enter the cavity. By definition, this equals the integral of $u(t)$ over time, therefore

$$-dV(t) = \int_0^t u(t')dt' = \frac{V}{\rho_{air}c^2}p(t), \qquad \Leftrightarrow \qquad P(s) = \frac{\rho_{air}c^2}{Vs}U(s).$$

Comparison of this relation with the last of Eqs. (3.22) is then straightforward: it is immediately seen that the quantity $\rho_{air}c^2/Vs$ is the acoustical equivalent of a capacitive impedance.

Analogously to the mechanical case, simple acoustic systems can be described as combinations of these elementary impedances. Consider a Helmholtz resonator driven by an external sound wave, as in Fig. 3.13(a). Both the inductive impedance associated with the tube and the resistance associated with the opening impede the same flow u, and are therefore in series. This flow u enters the cavity, so

Electrical		Mechanical		Acoustical	
Current i (A)		Velocity v (m/s)		Flow u (m^3/s)	
Voltage v (V)		Force f (N)		Pressure p (Pa)	
(Resistance) R	$\left(\frac{\text{Kg}\cdot\text{m}^2}{\text{s}}\right)$	(Damping) r	$\left(\frac{\text{Kg}}{\text{s}}\right)$	(Opening) R	$\left(\frac{\text{Kg}}{\text{m}^4\cdot\text{s}}\right)$
(Capacitance) $\frac{1}{sC}$		(Spring) $\frac{k}{s}$		(Cavity) $\frac{\rho_{air}c^2}{Vs}$	
(Inductance) $\frac{s}{L}$		(Mass) $m \cdot s$		(Bore) $\frac{\rho_{air}Ls}{S}$	

Table 3.1: Summary of analogies in electrical, mechanical and acoustical systems.

that the capacitance associated with the volume is in series with the other two. The resulting acoustic circuit is depicted in Fig. 3.13(b).

Table 3.1 summarizes the main analogies between electrical, mechanical, and acoustic systems, that we have discussed throughout this section.

3.4.1.3 Non-linearities

As mentioned previously, musical oscillators are typically non-linear: non-linearities must be present for a system to reach stable self-sustained oscillations, as in the case of persistently excited instruments (e.g., winds and strings). Non-linear elements may also be present in other systems in order to account for accurate modeling of interaction mechanisms. As an example, collisions between lumped masses are often described through a non-linear contact force.

The previous section has outlined the formal analogies between linear mechanical and electrical systems. It is possible to extend the analogy to the non-linear case. Consider the well known *Chua-Felderhoff* electrical circuit: this is a *RLC* circuit, made of a series connection of a resistor R, an inductor L and a capacitor C. The elements R and L are constant, while this is not the case for C. More precisely, the characteristic of the capacitance is a function of the voltage v, so that the system is described as follows:

$$\begin{aligned} v(q) &= \frac{1}{2v_0C_0}\left(q^2 + q\sqrt{q^2 + 4C_0^2v_0^2}\right), \quad \Leftrightarrow \quad C(v) = \frac{C_0}{\sqrt{1+\frac{v}{v_0}}}, \\ v(q) &+ R\dot{q}(t) + L\ddot{q}(t) = v_e(t), \qquad (v > v_0). \end{aligned} \tag{3.26}$$

The variable $q(t)$ stands for the charge on the capacitor, and $v_e(t)$ is an applied voltage. It is easily verified that $C(v) \sim C_0$ when $v \to 0$, i.e. the system is a linear *RLC* circuit in the limit of small oscillations. However, for larger voltage v this approximation does not hold, and $C(v)$, $q(v)$ behave as depicted in Fig. 3.14(a) and (b), respectively. Note that there is no easy way to translate the non-linear relation (3.26) into the Laplace domain, because the definition of impedance given in Sec. 3.4.1 assumes linearity of the circuit elements. The Chua-Felderhoff circuit has been extensively studied and is one of the classical systems used for exemplifying transition to chaotic behavior: when the

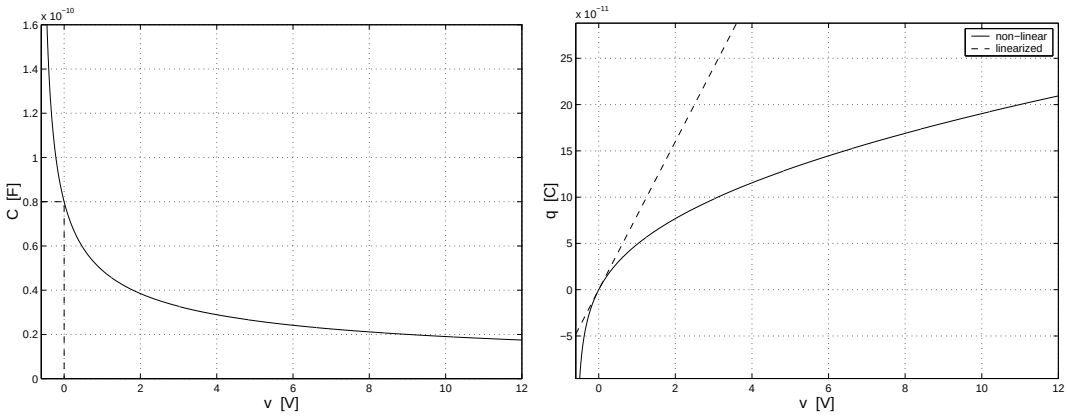

(a) (b)

Figure 3.14: Non-linear behavior of (a) capacitance $C(v)$ and (b) charge $q(v)$ in the Chua-Felderhoff circuit.

peak of the voltage generator is increased, the behavior of the charge $q(t)$ on the capacitor undergoes successive bifurcations.

The Chua-Felderhoff circuit finds some analogous counterparts in mechanical and acoustic systems. An example of non-linear elements is provided by an idealized contact model. In this model the contact restoring force is a non-linear[5] elastic force of the form

$$f(x(t)) = \begin{cases} kx(t)^\alpha, & x > 0, \\ 0, & x \leq 0, \end{cases} \tag{3.27}$$

where x is the penetration and k is an elastic constant. This model has been used for describing the compression characteristics of a piano hammer felt. The exponent α depends on the local geometry around the contact surface and typically takes values higher than 1. If the hammer is regarded as a lumped mass m and linear dissipation r is taken into account, then the complete model is described by the equation of motion

$$m\ddot{x}(t) + r\dot{x}(t) + kx(t)^\alpha = f_{ext}(t), \tag{3.28}$$

where f_{ext} is any external force acting on the hammer. This is formally identical to Eq. (3.26): the non-linear hammer is a series connection of a mechanical resistance r and inductance m with a non-linear capacitance. One obvious structural difference with the Chua-Felderhoff circuit is given by the different shape of the non-linearities.

[5] Note that the non-linear nature of Eq.(3.27) comes not only from the exponent α, but also from the conditional formulations for $x > 0$ and $x > 0$. In other words, f is non-linear even when $\alpha = 1$.

3.4.2 Modal synthesis

3.4.2.1 The second-order mechanical oscillator

The simplest possible resonating mechanical system that we can obtain using the lumped elements described in the last section is a second-order linear oscillator of the form

$$\ddot{x}^{(r)}(t) + g^{(r)}\dot{x}^{(r)}(t) + \left[\omega^{(r)}\right]^2 x^{(r)}(t) = \frac{1}{m^{(r)}} f_{ext}(t), \tag{3.29}$$

where $x^{(r)}$ is the oscillator displacement and f_{ext} represents any external driving force, while the parameters $\omega^{(r)} = k/m^{(r)}$ and $g^{(r)} = r/m^{(r)}$ are the oscillator center frequency and damping coefficient, respectively. With the analogies introduced in section 3.4.1, one can think of Eq. (3.29) as a series connection of the impedances m, r, k.

The resonating properties of such a one-dimensional model are summarized by its pitch $\omega^{(r)}$ and quality factor $q^{(r)} = \omega^{(r)}/g^{(r)}$. The parameter $g^{(r)}$ relates to the decay properties of the impulse response of system (3.29): specifically, the relation $t_e = 2/g^{(r)}$ holds, where t_e is the $1/e$ decay time of the impulse response.

M-3.7

Find the transfer function $H(s)$ between the driving force $F_{ext}(s)$ (input) and the displacement $X(s)$ (output) in equation (3.29). Study the frequency response and the impulse response.

If we want to produce more realistic and spectrally-rich sounds, a slightly more sophisticated model is obtained by parallel connection of N oscillators such as that of equation (3.29). By choosing a different center frequency $\omega_l^{(r)}$ ($l = 1 \dots N$) for each oscillator, it is possible to account for a set $\{\omega_l^{(r)}\}_{l=1}^N$ of partials of the resonator spectrum. A set of N decoupled modal resonators excited by the same external force can be described by means of a multivariable generalization of Eq. (3.29). In matrix form, this can be written as

$$\begin{bmatrix} \ddot{x}_1^{(r)}(t) \\ \vdots \\ \ddot{x}_N^{(r)}(t) \end{bmatrix} + \boldsymbol{G^{(r)}} \begin{bmatrix} \dot{x}_1^{(r)}(t) \\ \vdots \\ \dot{x}_N^{(r)}(t) \end{bmatrix} + \left[\boldsymbol{\Omega^{(r)}}\right]^2 \begin{bmatrix} x_1^{(r)}(t) \\ \vdots \\ x_N^{(r)}(t) \end{bmatrix} = \boldsymbol{m^{(r)}} f_{ext}(t), \tag{3.30}$$

where the matrices are given by

$$\boldsymbol{\Omega^{(r)}} = \begin{bmatrix} \omega_1^{(r)} & & \mathbf{0} \\ & \ddots & \\ \mathbf{0} & & \omega_N^{(r)} \end{bmatrix}, \quad \boldsymbol{G^{(r)}} = \begin{bmatrix} g_1^{(r)} & & \mathbf{0} \\ & \ddots & \\ \mathbf{0} & & g_N^{(r)} \end{bmatrix}, \quad \boldsymbol{m^{(r)}} = \begin{bmatrix} 1/m_1^{(r)} \\ \vdots \\ 1/m_N^{(r)} \end{bmatrix}. \tag{3.31}$$

3.4.2.2 The modal description

When a distributed resonating object is modeled as a chain of N masses connected with springs and dampers, the resulting system is composed of N coupled equations. However, the theory of modal analysis shows that it is generally possible find a transformation matrix $\boldsymbol{T} = \{t_{jl}\}_{j,l=1}^N$ which diagonalizes the system and turns it into a set of decoupled equations. The transformed variables $\{x_l^{(r)}\}_{l=1}^N$ are generally referred to as *modal displacements*. The displacement x_j and velocity v_j of the resonating object at a given point $j = 1 \dots N$ are then given by

$$x_j = \sum_{l=1}^{N} t_{jl} x_l^{(r)} \quad \text{and} \quad \dot{x}_j = \sum_{l=1}^{N} t_{jl} \dot{x}_l^{(r)} \tag{3.32}$$

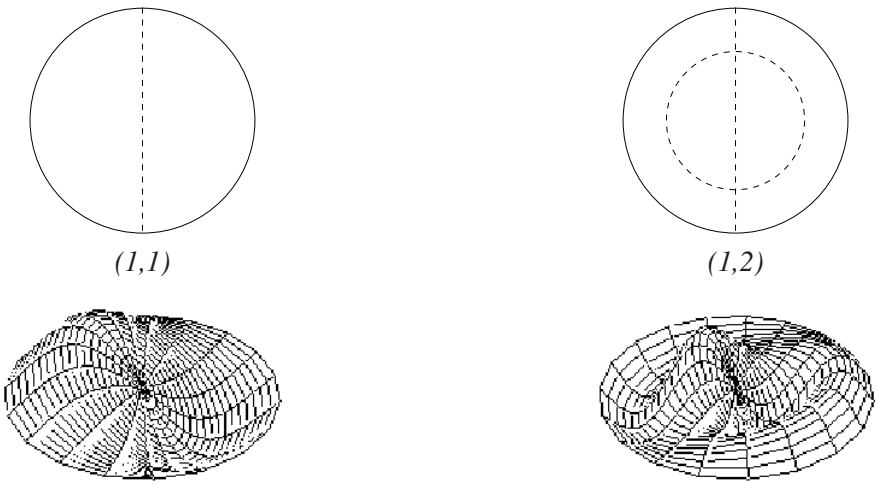

Figure 3.15: A circular membrane displaced from its rest position according to the spatial shape of mode(1,1) (left) and mode(1,2) (right).

The modal description given by Eqs. (3.30), (3.32) provides a high degree of controllability. The damping coefficients $g_l^{(r)}$ control the decay times of each exponentially-decaying mode of the resonator. The frequencies $\omega_l^{(r)}$ can be chosen to reproduce spectra corresponding to various geometries of one-, two- and three-dimensional resonators. As an example, the first N resonances of a cavity can be mapped into the modal frequencies of the N oscillators, and morphing between different shapes can be obtained by designing appropriate trajectories for each of these resonances.

In this context the quantities $m_l^{(r)}$ are often referred to as *modal masses*, while the quantities $1/m_l^{(r)}$ are referred to as *modal weights*. Note that by allowing the modal masses to vary for each oscillator, the matrix $\boldsymbol{m^{(r)}}$ can be generalized to give control on the amounts of energy provided to each oscillator. This permits simulation of position-dependent interaction, in that different interaction points excite the resonator modes in different ways.

Figure 3.15 shows a membrane which is displaced from its rest position in such a way that only one single mode is set into vibration. The distance of each point of the membrane from the "rest plane" is proportional to the weighting factor $1/m^{(r)}$ of the mode at this position. Note that the intersections of the mode–shape with the rest plane (i.e., the *nodal lines*) remain fixed during the entire cycle of the modal vibration. Therefore, the modal weights at these positions are 0 (equivalently, the modal masses tend to infinity). Correspondingly, an external force applied at these node lines does not excite the mode at all. In order for the resonator model (3.30) to account for such a situation, the weights $1/m_l^{(r)}$ must be made position-dependent. In other words, the $(N \times 1)$ matrix $\boldsymbol{m^{(r)}}$ must be generalized by defining a $(N \times N)$ matrix $\boldsymbol{M^{(r)}}$, whose element (l, j) is the modal weight of mode l at interaction point j.

In the case of a system of N point masses with linear interaction forces, modal parameters are exactly found through standard matrix calculations. Most systems of interest of course do not fit these assumptions. In some cases the differential equations of distributed systems can be solved analytically, giving the modal parameters; this holds for several symmetrical problems as circular or rectangular membranes. Alternatively, either accurate numerical simulations (e.g. wave-guide mesh

methods) or "real" physical measurements can be used. Impulse responses computed (or recorded) at various interaction points then form a basis for the extraction of modal parameters. The acoustic "robustness" of the modal description allows convincing approximations on the basis of microphone-recorded signals of e.g. an object struck at different points, despite all the involved inaccuracies: spatially distributed interaction, as well as wave distribution through air, provide signals that are quite far from impulse/frequency responses at single points.

3.4.3 Numerical methods

Unlike waveguide structures, the lumped models described so far are developed in the continuous-time domain, and are in general described through sets of ODEs. In order to be implemented as numerical algorithms for sound synthesis, the differential equations have to be discretized in an efficient and effective manner. In most cases, a trade-off has to be found between accuracy of the discretization technique and efficiency of the resulting algorithms.

3.4.3.1 Impulse invariant method

When dealing with linear systems, such as the lumped elements of Sec. 3.4.1, the most elementary numerical technique is sampling. Given the admittance $\Gamma(s)$ of a linear system (in a mechanical lumped system, this corresponds to defining the input as the driving force and the output as the resulting velocity), its inverse Laplace transform $\gamma(t)$ is the continuous-time impulse response. The linear system can thus be digitized by defining the discrete response as $\gamma_d[n] := T_s\gamma(nT_s)$, i.e. by sampling $\gamma(t)$. This technique is widely used in the context of digital filter design, and it is usually termed the *Impulse Invariant Method*. One quality of the method is that stability is guaranteed at any sampling rate: if p_c is a pole of the continuous-time response, the corresponding pole of the discrete-time response is given by $p_d = e^{p_c T_s}$. This implies that if $\mathrm{Re}(p_c) < 0$, then $|p_d| < 1$, i.e. the discrete-time pole lies inside the unit circle. On the other hand, a drawback of the method is *aliasing*. It is known that the discrete-time response Γ_d is obtained as a periodization of the continuous one:

$$\Gamma_d(e^{j\omega}) = \sum_{k=-\infty}^{+\infty} \Gamma\left(\frac{j\omega}{T_s} + j\frac{2k\pi}{T_s}\right). \tag{3.33}$$

As a consequence, any Γ whose bandwidth is wider than $F_s/2$ introduces spurious components in Γ_d.

3.4.3.2 Mappings "s-to-z"

An approach alternative to sampling amounts to replacing time derivatives with finite differences, thus turning the differential equations directly into difference equations. Since in the Laplace domain the derivation operator is turned to a multiplication by s, and since in the Z domain the unit delay is turned into a multiplication by z^{-1}, approximating derivatives with finite differences corresponds in the frequency domain to finding appropriate *s-to-z mappings*. Let $s = g(z)$ be such a mapping, then the discrete-time response is found as $\Gamma_d(z) = \Gamma\left(g(z)\right)$.

The simplest possible mapping is obtained by replacing the derivative with an incremental ratio.

Let $x(t)$ be a smooth function of time, then

$$\begin{aligned} &\frac{d}{dt}x(t_n) := \lim_{h\to 0_+} \frac{x(t_n) - x(t_n - h)}{h} \approx \frac{x(t_n) - x(t_{n-1})}{T_s} := \delta_t x[n], \\ &\Rightarrow \qquad s \approx \frac{1 - z^{-1}}{T_s} := g_1(z). \end{aligned} \tag{3.34}$$

where $t_n = nT_s$. The mapping $g_1(z)$ is known in numerical analysis as the *backward Euler method*. The adjective "backward" is used because the first derivative of x at time n is estimated through the values of x at time n and $n-1$. Note that the method is *implicit*, since it turns a generic first-order differential equation $\dot{x}(t) = f(x(t), t)$ into a difference equation of the form $x[n] = f_d(x[n], x[n-1], n)$, in which $x[n]$ depends implicitly on itself through f_d. Higher-order derivatives can be estimated through iterate application of Eq. (3.34). The second derivative is computed as

$$\frac{d^2}{dt^2}x(t_n) \approx \frac{1}{T_s}\left[\delta_t x[n] - \delta_t x[n-1]\right] = \frac{x(t_n) - 2x(t_{n-1}) + x(t_{n-2})}{T_s^2}. \tag{3.35}$$

M-3.8

Take the mechanical oscillator (3.29) and discretize it with the Euler method $g_1(z)$. Study the frequency response and the impulse response, compare them with those found in M-3.7.

A centered estimate is also often used in combination with the backward Euler method. In this case the second derivative is computed as:

$$\frac{d^2}{dt^2}x(t_n) \approx \frac{x(t_{n+1}) - 2x(t_n) + x(t_{n-1})}{T_s^2}. \tag{3.36}$$

One can verify that using this estimate on a second-order ODE leads to an *explicit* difference equation.

A second, widely used s-to-z mapping is provided by the *bilinear transform*. Like the backward Euler method, it can be seen as a finite approximation of the time derivative, but in this case the incremental ratio is assumed to approximate the mean value of $\dot{x}$ at time instants t_n and t_{n-1}:

$$\begin{aligned} &\frac{x(t_n) - x(t_{n-1})}{T_s} \approx \frac{\dot{x}(t_n) + \dot{x}(t_{n-1})}{2}, \\ &\Rightarrow \qquad s \approx 2F_s\frac{1 - z^{-1}}{1 + z^{-1}} := g_2(z). \end{aligned} \tag{3.37}$$

The mapping $g_2(z)$ is known in numerical analysis as the one-step *Adams-Moulton method*. Like the backward Euler method, it is implicit.

M-3.9

Take the mechanical oscillator (3.29) and discretize it with the bilinear transform $g_2(z)$. Study the frequency response and the impulse response, compare them with those found in M-3.7 and M-3.8.

3.4.3.3 Accuracy, stability

A comparison between the first estimate in Eq. (3.37) and the first in Eq. (3.34), gives the intuition that the bilinear transform provides a more accurate approximation than the Euler method. A rigorous analysis would show that the order of accuracy of the bilinear transform is two, while that of the backward Euler method is one.

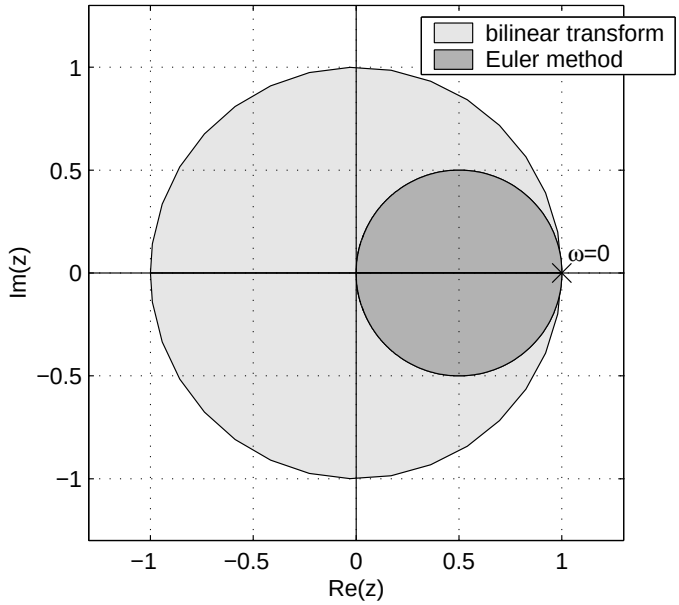

Figure 3.16: Images of the vertical axis $s = j\omega$ (solid lines) and of the left-half s-plane (gray regions) using the backward Euler method g_1 and the bilinear transform g_2.

Another way of comparing the two techniques consists in studying how the frequency axis $s = j\omega$ and the left-half plane $\mathrm{Im}(s) < 0$ are mapped by $g_{1,2}$ into the discrete domain. This gives information on the stability and accuracy properties of $g_{1,2}$. Figure 3.16 provides an illustration, from which two remarks can be made. First, both the methods define one-to-one mappings from $s = j\omega$, onto the two circles plotted in Fig. 3.16 (solid lines): therefore no frequency aliasing is introduced. Second, both the methods are stable, since the left-half s-plane is mapped inside the unit circle by both g_1 and g_2.

However we also see that both the mappings introduce frequency warping, i.e. the frequency axis is distorted. One can verify that the bilinear transform g_2 maps the $s = j\omega$ axis exactly onto the unit circle $z = e^{j\omega_d}$, and the direct mapping $\omega_d = 2 \cdot \arctan(\omega)$ can be defined between the continuous frequencies ω and the discrete frequencies ω_d. At low frequencies, ω_d increases almost linearly with ω, while higher frequencies are progressively compressed (warped) and the Nyquist frequency πF_s is mapped to the point $z = -1$. Warping is the main drawback of the bilinear transform.

The Euler method maps the $s = j\omega$ axis onto the circle of radius $1/2$ centered at $z = 1/2$. Therefore no direct mapping is found from ω to ω_d. The function g_1 can be said to "doubly" warp the frequency axis: there is a progressive warping in the direction of increasing frequency (similarly to the bilinear transform), but there is also warping normal to the frequency axis. As far as stability is concerned, Fig. 3.16 shows that the poles of the discrete-time system obtained with g_1 are more "squeezed" inside the unit circle than the ones obtained with g_2. Furthermore, it can happen that continuous-time poles with positive real-part are turned by g_1 into discrete-time poles with modulus less than unity: in other words g_1 can turn unstable continuous systems into stable discrete systems. This *numerical damping* is a second major drawback of the Euler method. An example of such a damping property of the Euler method is provided in Sec. 3.5 (see in particular figure 3.21).

3.4.3.4 Wave digital filters

The bilinear transform finds application in Wave Digital Filters (*WDF*) theory. These structures are the digital equivalent of the lumped circuits described in Sec. 3.4. Wave digital filters are constructed in two steps. The first step amounts to converting the continuous-time lumped circuits in wave variables. In this context, the definition of wave variables is identical to that used for waveguides models (see Eq. (3.12) in Sec. 3.3), namely:

$$f^+ = \frac{f + Z_0 v}{2}, \qquad f^- = \frac{f - Z_0 v}{2}, \tag{3.38}$$

where the mechanical Kirchhoff variables force f and velocity v have been used for clarity. The only and fundamental difference with Eq. (3.12) is that in this context Z_0 is a reference impedance that can be given any value and has no direct physical interpretation. The variables $f^\pm$ themselves do not have a clear physical interpretation since in a lumped model they cannot be easily interpreted as traveling waves. Therefore in this context the Eqs. (3.38) have to be regarded as a mere change of coordinates.

Consider one of the elementary lumped elements analyzed in Sec. 3.4 and its associated impedance $Z(s)$. Then the new continuous-time variables $f^\pm$ are related to each other through a *reflectance* $R(s)$:

$$F(s) = Z(s)V(s), \quad \Rightarrow \quad F^-(s) = R(s)F^+(s), \quad \text{with} \quad R(s) := \frac{Z(s) - Z_0}{Z(s) + Z_0}. \tag{3.39}$$

The second step in WDF design is the discretization of $R(s)$. The equivalent wave digital filter $R_d(z)$ is then obtained using the bilinear transform: $R_d(z) = R(g_2(z))$. Note that since the reference impedance Z_0 can be given any value, this provides an additional degree of freedom for the design of R_d. In particular, Z_0 can be chosen such that R_d has no delay-free paths from input to output. This is an essential requirement for guaranteeing computability when connecting more than one element. A simple example will help clarify this concept: consider a mass mass m and its associated impedance $Z(s) = ms$, as found in Sec. 3.4. Then, from Eq. (3.39) the corresponding reflectance is $R(s) = (ms - Z_0)/(ms + Z_0)$. Choosing $Z_0 = 2F_s m$ leads to the interesting result

$$R(s) = \frac{s - 2F_s}{s + 2F_s}, \quad \Rightarrow \quad R_d(z) = -z^{-1}, \tag{3.40}$$

so that no delay-free path is present in the wave digital filter R_d. This simple example gives us the intuition that lumped elements can be described using wave digital filters, and connected to each other by *adapting* impedances in order to avoid the occurrence of delay-free computational loops.

3.4.4 Computability issues

The discussion of wave digital filters in the last section has addressed the problem of non-computable loops in that particular context: wave variables rather than Kirchhoff variables are used to describe the components of the equivalent circuit, every component is treated as a scattering element with a reference impedance, and different components are connected to create the complete computational structure. Wave methods can be said to be *local*, since non-computable paths are avoided by adapting the reference impedances of each element. However, more severe computability problems can arise when simulating dynamic exciters, since the linear equations used to describe the system dynamics are tightly coupled with some non-linear map.

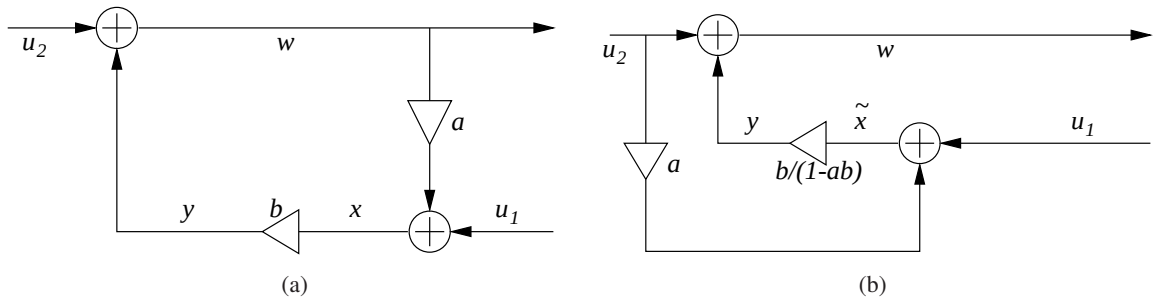

Figure 3.17: A linear system; (a) delay-free path, (b) equivalent realization with no delay-free paths.

3.4.4.1 The delay-free loop problem

Let us start with a trivial example in order to focus the problem that we want to deal with. Consider the system depicted in Fig. 3.17(a). It is easily verified that the discrete-time system can be written as

$$\begin{cases} w[n] = \tilde{w}[n] + y[n], & \text{with} \quad \tilde{w} = u_2, \\ x[n] = \tilde{x}[n] + ay[n], & \text{with} \quad \tilde{x} = u_1 + au_2, \\ y[n] = f(x[n]) = bx[n], & \Rightarrow \quad y[n] = b[u_1[n] + au_2[n] + ay[n]]. \end{cases} \tag{3.41}$$

where we have defined tilded variables $\tilde{w}$ and $\tilde{x}$ than only depend on the external inputs $u_{1,2}$, and are therefore known at each time n. The function f is a linear map (scaling by a constant b).

Note that a delay-free computational loop connects y to x, in particular the last of Eqs. (3.41) shows that y depends implicitly on itself. It is easy, however, to rearrange the computation in order to solve this problem: the last of Eqs. (3.41) can be inverted, yielding

$$y[n] = f(x[n]), \quad \longmapsto \quad y[n] = h(\tilde{x}[n]) = \frac{b}{1-ab}[u_1[n] + au_2[n]]. \tag{3.42}$$

The new map h relates y to the computable vector $\tilde{x}$. Therefore, an equivalent realization of the system is obtained as shown in Fig. 3.17(b). The key point in this example is that f is linear, which allows explicit inversion of the last equation in (3.41).

This simple example is an instance of the so-called *delay-free loop* problem. In the linear case the literature of digital signal processing provides techniques for the restoring computability by rearrangement of the structure. However we are here interested in the non-linear case, since non-linear elements are almost always present in physical models. In section 3.2.1 we have stated that non-linear elements are typically associated to excitation mechanisms. Figure 3.18 depicts a typical structure which is found when "zooming" inside the excitation block of a musical instrument (cfr. Fig. 3.1). The elements denoted by **L** and **NL** represent a linear and a non-linear block, respectively. More precisely, **L** contains a linear filter that accounts for the system dynamics in terms of lumped elements, while **NL** contains a non-linear multiple-input, multiple-output (*MIMO*) map $\boldsymbol{f}(\cdot)$. Both of these blocks take exciting actions $\boldsymbol{u}_2$ and the resonator variables $\boldsymbol{u}_1$ as inputs, and they are connected to each other in a feedback loop. This representation does not seem to be restrictive for acoustic models.

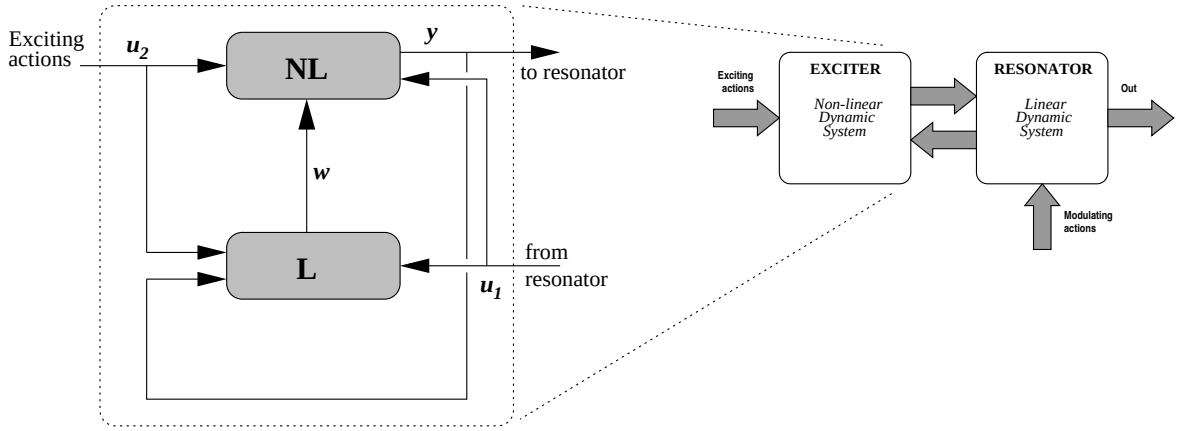

Figure 3.18: Typical structure of a non-linear exciter.

Without any loss in generality, we assume in the following that the non-linear map $\boldsymbol{f}$ depends on a linear combination $\boldsymbol{x}$ of its inputs $(\boldsymbol{w}, \boldsymbol{u}_1, \boldsymbol{u}_2)$. Thus, the continuous-time system of Fig. 3.18 is described through the equations

$$\begin{cases} \dot{\boldsymbol{w}}(t) = \boldsymbol{A}\boldsymbol{w}(t) + \boldsymbol{B}\boldsymbol{u}(t) + \boldsymbol{C}\boldsymbol{y}(t), \\ \boldsymbol{x}(t) = \boldsymbol{D}\boldsymbol{w}(t) + \boldsymbol{E}\boldsymbol{u}(t) + \boldsymbol{F}\boldsymbol{y}(t), \\ \boldsymbol{y}(t) = \boldsymbol{f}\left(\boldsymbol{x}(t)\right), \end{cases} \tag{3.43}$$

where the vector $\boldsymbol{u} = [\boldsymbol{u}_1, \boldsymbol{u}_2]^T$ collects all the external inputs to the exciter.

When equations (3.43) are discretized using a linear numerical method (e.g. those described in the previous section), the discrete-time system takes the form

$$\begin{cases} \boldsymbol{w}[n] = \tilde{\boldsymbol{w}}[n] + \tilde{\boldsymbol{C}}\boldsymbol{y}[n], \\ \boldsymbol{x}[n] = \tilde{\boldsymbol{x}}[n] + \boldsymbol{K}\boldsymbol{y}[n], \\ \boldsymbol{y}[n] = \boldsymbol{f}\left(\boldsymbol{x}[n]\right) = \boldsymbol{f}\left(\tilde{\boldsymbol{x}}[n] + \boldsymbol{K}\boldsymbol{y}[n]\right), \end{cases} \tag{3.44}$$

where the vectors $\tilde{\boldsymbol{w}}$ and $\tilde{\boldsymbol{x}}$ are computable vectors, i.e. they are linear combinations of $\boldsymbol{u}$ and past values of $\boldsymbol{w}$ and $\boldsymbol{y}$. Note that this system generalizes the linear example (3.41).

Equations (3.44) show that if $\boldsymbol{K}$ is non null, there is a delay-free path connecting $\boldsymbol{y}$ to $\boldsymbol{x}$ with $\boldsymbol{K}$ "weighing" this path. Note that explicit expressions for the vectors $\tilde{\boldsymbol{w}}$, $\tilde{\boldsymbol{x}}$ and the matrices $\tilde{\boldsymbol{C}}$, $\boldsymbol{K}$ depend on what discretization method is used, but the overall system structure (3.44) remains the same. In particular, the matrix $\boldsymbol{K}$ is always non null when an implicit linear method is used.

3.4.4.2 Approaches

It should be clear that in the non-linear case one cannot perform a rearrangement such as in (3.41), because the last equation in (3.44) is in general not analytically invertible. The question is then how

to deal with the delay-free loop problem in the non-linear case.

- One can use an *explicit* numerical method, that produces a system of difference equations (3.44) in which $\tilde{\boldsymbol{C}}$ and $\boldsymbol{K}$ are null. This choice solves the computational problem but can introduce more severe artifacts in the numerical system: explicit methods have lower orders of accuracy with respect to implicit methods, and more importantly are not unconditionally stable, i.e. are not stable for any sampling frequency F_s and for any values of the system parameters. A sound synthesis algorithms that explodes can be very unpleasant.

M-3.10

Take the mechanical oscillator (3.29) and discretize it with the Euler method $g_1(z)$ in conjunction with the centered estimate (3.36). Verify that the difference equation is explicit, study the frequency response and the impulse response, compare them with those found in M-3.7, M-3.8, and M-3.9. Study the poles of the digital system and veify that it can become unstable.

- A rudimentary solution, that is nonetheless often met in the literature of physical modeling, amounts to inserting a fictitious delay element in the feedback loop, or in other words to assume that on the right-hand side of the last equation in (3.44) the approximation $\boldsymbol{y}[n] \approx \boldsymbol{y}[n-1]$ holds. In practice this is a variant of the previous approach: instead of using an explicit method from the beginning, one makes the computation explicit *a posteriori*, throug the insertion of a z^{-1} element. While this "trick" can be acceptable at significantly high sampling rates, the insertion of such a delay element can again deteriorate the accuracy and stability properties of the numerical system. Even worse, in this case one cannot determine analytically the stability range of the system.

- Numerical analysis provides a plethora of iterative methods to find solutions of non-linear systems of algebraic equations: examples of such methods include fixed-point iteration and Newton iteration, and each of them requires specific hypothesis on the non-linear system to hold. These methods can be exploited for our problem: at each time n one knows $\tilde{\boldsymbol{x}}[n]$ and can estimate $\boldsymbol{y}[n]$ by finding a zero of $\boldsymbol{g}_{\tilde{x}}(\boldsymbol{y}) = \boldsymbol{f}(\tilde{\boldsymbol{x}} + \boldsymbol{K}\boldsymbol{y}) - \boldsymbol{y}$. In other words, at each time n one can estimate numerically a (non-linear) function $\boldsymbol{y} = \boldsymbol{h}(\tilde{\boldsymbol{x}})$. If we go back and look at equation (3.42) we see what we are doing here: since we cannot invert $\boldsymbol{f}$ analytically and find $\boldsymbol{h}$ globally (as we did in the linear case) we estimate it *locally*, around a given value $\tilde{\boldsymbol{x}}[n]$.
  Using an iterative solver is advantageous over the previous approaches in that we can exploit the accuracy and stability properties of an implicit method without introducing additional numerical errors in the system. One major drawback, however, is that one does not know in advance the number of iterations that are needed for the solver to converge to the solution $\boldsymbol{y}[n]$: this can be a problem for real-time applications, where one wants to know the time needed to compute one sound sample.

- *Predictor-corrector* methods are a class of numerical schemes that are well suited for solving non-linear implicit difference equations. The basic idea is rather simple to understand: if the starting point of the search is close enough to the solution, fixed-point iteration (or any other iterative solver) will converge quickly. Predictor-corrector schemes then use an explicit numerical method (the predictor) to provide an initial guess of the new value; the true new value is found using an implicit method (the corrector) and an iterative solver (typically fixed-point iteration). Numerical analysis shows that normally a very low number of iterations provide acceptable accuracy. These schemes are therefore a valid alternative to the previous approach,

quantity	symbol	unit
Reed tip displ.	$y_L(t)$	m
Tip rest position	y_0	m
Max. tip displacement	y_m	m
Reed tip opening	$h(t) = y_m - y_L(t)$	m
Reed mass/area	μ	Kg/m^2
Effective reed area	S_d	m^2
Reed resonance freq.	ω_0	rad/s
Reed damping	g	3000 s^{-1}
Mouth pressure	p_m	Pa
Mouthpiece pressure	$p(t)$	Pa
Pressure drop	$\Delta p(t) = p_m - p(t)$	Pa
Mouthpiece flow	$u(t)$	m^3/s
Flow through the slit	u_f	m^3/s
Sound speed in air	$c = 347$	m/s
Air density	$\rho_{air} = 1.14$	Kg/m^3
Bore cross section	S	m^2
Bore wave impedance	$Z_0 = \rho_{air} c/S$	Kg/m^{4}s
Bore length	L_{bore}	m
Press. wave from the bore	$p^-(t)$	Pa
Press. wave to the bore	$p^+(t)$	Pa

Table 3.2: Symbols used throughout the section.

especially because the number of iterations (usually 1 or 2) of the corrector are set in advance. Note however that predictor-corrector schemes have been very rarely used in the literature of physical modeling.

3.5 A full example: the clarinet

In this last section we apply the modeling approaches discussed so far to a concrete example of musical instrument. There is a number of reasons for choosing the clarinet: it is a widely studied instrument in the literature of musical acoustics, and much is known of its functioning; it provides a paradigmatic example of self-sustained oscillations initiated by a non-linear persistent excitation mechanism; last but not least, it can be modeled with relatively simple structures. All in all, the clarinet constitues an ideal candidate for exemplifying the construction of a non-trivial physical model of a musical instrument.

Table 3.2 summarizes the main variables and parameters used throughout this section. The instrument can be decomposed according to the general scheme summarized in figure 3.1. The exciter is represented by the reed-mouthpiece system, that acts as a non-linear pressure-controlled valve, and determines the drop Δp between the pressure p_m inside the player's mouth and the pressure p inside the mouthpiece. The resonator coincides with the acoustical bore, and can be subdivided into sub-blocks, such as bell and holes.

3.5.1 Functional blocks

3.5.1.1 Resonator: the bore

As a first approximation, the clarinet bore can be assumed to be cylindrical. Therefore the most basic model for the bore can be obtained using a single waveguide section, that simulates plane wave propagation, and a perfect reflection at the open end (bell). According to this oversimplified model, the pressure wave p^- entering the mouthpiece from the bore is given by

$$p^-[n] = -p^+[n - 2m_{bore}] \qquad \Leftrightarrow \qquad P^-(z) = -z^{-2m_{bore}} P^+(z). \tag{3.45}$$

The number $2m_{bore}$ of unit delays for the waveguide is related to the bore length L_{bore} and to the sampling frequency F_s through the equation $L_{bore} = c \cdot m_{bore}/F_s$.

A slightly more accurate model is obtained by taking into account the radiating properties of the bell. The bell itself can be seen as a low-pass filter, that reflects low frequencies back inside the bore, and radiates frequencies above its cutoff. Typical values for the cutoff frequency are around 1500 Hz. Let $R_d(z)$ be the transfer function of such a low-pass filter: then the pressure wave p^- that enters the mouthpiece from the bore is given by

$$p^-[n] = -(r_d * p^+)[n - 2m_{bore}] \qquad \Leftrightarrow \qquad P^-(z) = -z^{-2m_{bore}} R_d(z) P^+(z). \tag{3.46}$$

The portion that is radiated from the bell is instead given by

$$p_{\text{out}}[n] = p^+[n-m_{bore}]+(r_d*p^+)[n-m_{bore}] \qquad \Leftrightarrow \qquad P_{\text{out}}(z) = z^{-m_{bore}}[1+R_d(z)]P^+(z). \tag{3.47}$$

M-3.11

Construct the WG bore model according to equation (3.46), as a function that takes a pressure wave $p^+[n]$ from the mouthpiece and returns a pressure wave $p^-[n]$ back to the mouthpiece.

Further refinements to this model should include losses, that can be incorporated in the model according to the techniques described in section 3.3. Fractional-delay filters should also be incorporated in the model in order to allow for fine tuning of the bore length L_{bore} (note that so far we have assumed that $L_{bore}F_s/c = m_{bore}$ with m_{bore} integer, which clearly implies a crude quantization of L_{bore}). Finally, holes can be incorporated into the model through scattering filters connected through 3-port junctions to the main waveguide structure.

3.5.1.2 Excitation: the reed

We turn now to the exciter block, which corresponds to the reed-mouthpiece system and is schematically represented in figure 3.19.

The reed dimensions are small with respect to typical wavelengths in the resonator, thus pressure can be thought of as constant along the reed internal surface; under normal playing conditions, the first mode of the reed-mouthpiece-lip system is well above the main frequency component of the pressure signal that drives it; oscillations occur mainly in the vertical direction, and as a first approximation a single degree of freedom (i.e. the reed tip vertical displacement y_L) can be assumed.

These considerations justify the choice of a *lumped* modeling approach for the reed. Many authors have approximated the reed as a lumped second-order mechanical oscillator, driven by the pressure drop Δp between mouth and mouthpiece:

$$m\ddot{y}_L(t) + r\dot{y}_L(t) + k[y_L(t) - y_0] = S_d \Delta p(t), \tag{3.48}$$

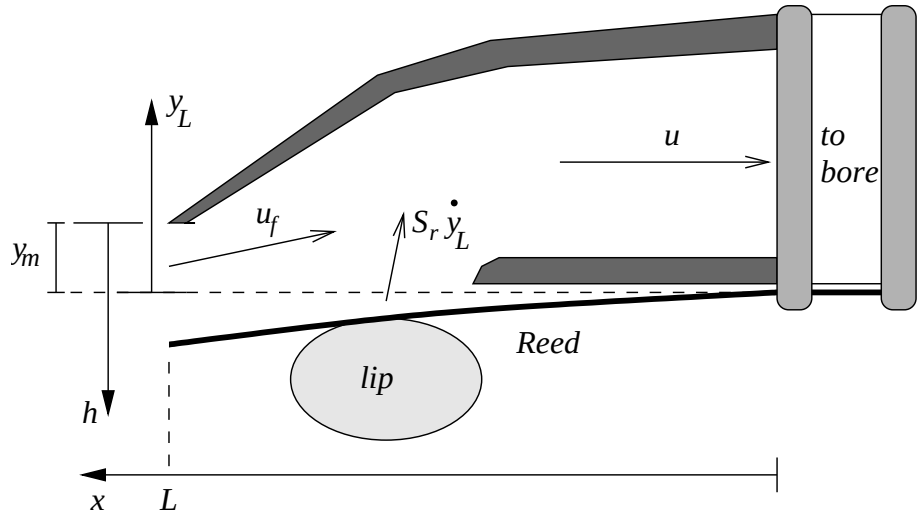

Figure 3.19: Schematized representation of the reed-mouthpiece system.

where m, r, k are the reed mass, damping, and spring constant, respectively. The parameter S_d is an effective driving surface on which the pressure Δp acts. In the Laplace domain, Eq. (3.48) can be rewritten as

$$Y_L(s) - y_0 = H_r(s)\Delta P(s), \quad \text{with} \quad H_r(s) = \frac{1}{\mu}\frac{1}{s^2 + gs + \omega_0^2}. \tag{3.49}$$

Therefore, H_r is the transfer function between Δp and the reed relative displacement. The parameter $\mu = m/S_d$ is the effective mass/area ratio, $g = r/m$ is the damping coefficient and $\omega_0 = \sqrt{k/m}$ is the resonance of the oscillator.

The phenomenon of reed beating (i.e. complete closure of the reed) is usually incorporated in the lumped model in a non-physical way, by imposing a "stop" when the reed tip reaches its maximum allowed displacement y_m. Equation (3.48) is thus turned into

$$\begin{cases} m\ddot{y}_L(t) + r\dot{y}_L(t) + k(y_L(t) - y_0) = S_d\Delta p(t), & \text{for} \quad y_L < y_m, \\ y_L(t) = y_m \quad \text{and} \quad \dot{y}_L(t) = 0, & \text{for} \quad y_L \geq y_m. \end{cases} \tag{3.50}$$

Once the mechanical part has been modeled, the relation between the reed opening and the airflow through the slit u_f has to be found. As a first approximation, the pressure drop Δp can be assumed to obey the equation

$$\Delta p(t) = f(u_f(t), h(t)) = A^{-\alpha}\text{sgn}[u_f(t)]\frac{|u_f(t)|^\alpha}{h(t)^2}, \tag{3.51}$$

which is derived from the Bernoulli law.[6]

Equations (3.50) and (3.51) relate quantities at the reed slit. A third equation relates the flow u_f at the slit to the total flow u inside the instrument:

$$u(t) = u_f(t) + u_r(t), \quad \text{with} \quad \begin{cases} u_f(t) = \frac{1}{Z_0}(p^+(t) - p^-(t)), \\ u_r(t) = S_r\dot{y}_L(t). \end{cases} \tag{3.52}$$

[6]The Bernoulli law, which holds for incompressible non-viscous fluids and in stationary conditions, states that the relation $u_f = A \cdot x \cdot \Delta p^{1/2}\text{sgn}(\Delta p)$ holds through an aperture of width x. Some authors adopt for the single reed the generalized equation $u_f = [A \cdot x\Delta p^{1/2}\text{sgn}(\Delta p)]^{1/\alpha}$, with an experimentally determined value $\alpha = 3/2$.

This equation states that the total flow inside the instrument is affected by an additional component $u_r(t)$, induced by the reed motion and proportional to the reed tip velocity. The quantity S_r is the effective flow surface of the reed, and is not necessarily equal to S_d.

3.5.2 The quasi-static approximation

In a single reed instrument the fundamental regime of oscillation is governed by the first resonance frequency of the pipe, and typical values for the reed mechanical resonance ω_0 are well above this pipe resonance and the frequency band of $p(t)$.

It is therefore reasonable to assume a *quasi-static approximation* for the reed response, in which the exact relation $(Y_L(s) - y_0) = H_r(s)\Delta P(s)$ is substituted by the simpler

$$(Y_L(s) - y_0) = H_r(0)\Delta P(s) := \frac{1}{K_a}\Delta P(s) \tag{3.53}$$

Since $H_r(0)$ is a scalar rather than a filter, equation (3.53) assumes that the reed motion is in phase and proportional to the pressure drop. The quantity K_a is usually termed reed *stiffness per unit area*. One can easily verify from equation (3.49) that $K_a = mu\omega_0$.

Using Eq. (3.53), the reed opening h is computed as

$$h(t) = y_m - y_0 - \frac{\Delta p(t)}{K_a} = h_0 - \frac{\Delta p(t)}{K_a},$$

where $h_0 = y_m - y_0$ is the rest opening of the reed tip. Substituting this relation into equation (3.51) one finds

$$u_f(t) = \begin{cases} A \cdot \text{sgn}[\Delta p(t)] \cdot |\Delta p|^{1/\alpha} \left(h_0 - \dfrac{\Delta p(t)}{K_a}\right)^{2/\alpha} & \text{for} \quad \Delta p < h_0 K_a, \\ 0, & \text{for} \quad \Delta p \geq h_0 K_a. \end{cases} \tag{3.54}$$

Equation (3.54) provides a relation between u_f and Δp in which the reed dynamics has been removed. Figure 3.20(a) shows the plot of this relation. For low Δp values, u_f increases until a maximum at $\Delta p = h_0 K_a/3$. Then the flow starts to drop due to reed closure, and reaches the value $u_f = 0$ at $\Delta p = h_0 K_a$. Beyond this value the reed is completely closed.

The non-linear map (3.54 can be used to construct a quasi-static reed model. If wave variables $p^{\pm}$ are introduced, the non-linearity can be turned in a new one in which p^+ depends on p^- through a non-linear reflection function R_{nl}, i.e. $p^+ = R_{nl}(p^-)$. This is depicted in Fig. 3.20(b).

M-3.12

Construct the quasi-static reed model according to equation (3.54), as a function that takes a pressure wave $p^-[n]$ from the bore and returns a pressure wave $p^+[n]$ back to the bore.

Despite its simplicity, the quasi-static model is able to capture the basic non-linear mechanisms of self-sustained oscillations in a single reed instrument. Due to its compactness and low number of parameters, this model has been also used for sound synthesis purposes.

M-3.13

Implement the complete quasi-static clarinet model: using the functions developed in M-3.11 and M-3.12, write an audio cycle in which the system is initialized with a certain mouth pressure p_m and evolves freely. Plot the signal and its spectrogram.

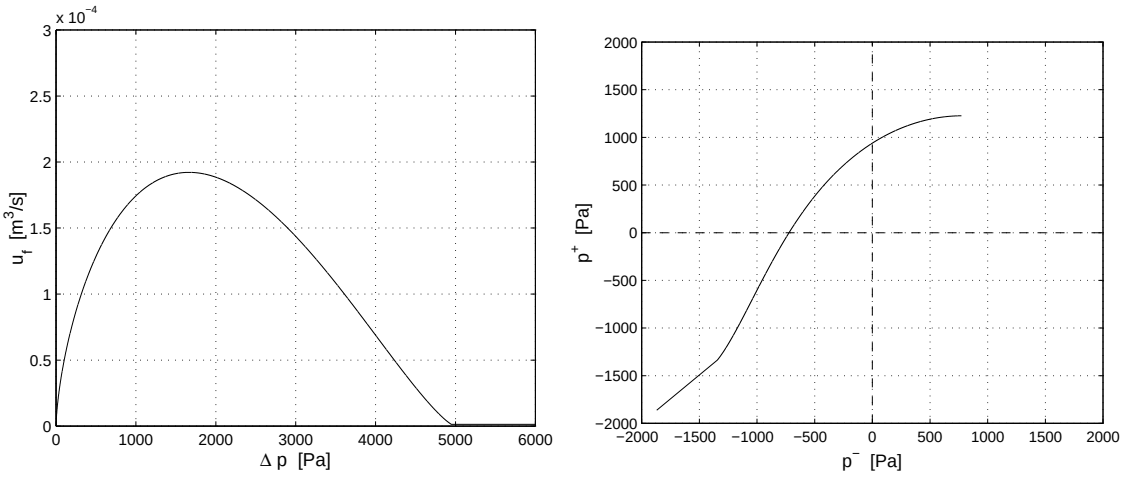

(a) (b)

Figure 3.20: Quasi-static approximation of a single reed; (a) u_f versus Δp and (b) rotated mapping $p^+ = R_{nl}(p^-)$.

3.5.3 The dynamic reed model

In order to obtain more realistic behavior from the clarinet model we want now to use the dynamic lumped reed formulation described in section 3.5.1. The continuous-time system described by equations (3.50, 3.51, 3.52) can be restated in vector formulation as

$$\begin{cases} \dot{\boldsymbol{w}}(t) &= \boldsymbol{A}\boldsymbol{w}(t) + \boldsymbol{B}\boldsymbol{u}(t) + \boldsymbol{C}\Delta p(t), \\ \boldsymbol{x}(t) &= \boldsymbol{D}\boldsymbol{w}(t) + \boldsymbol{E}\boldsymbol{u}(t) + \boldsymbol{F}\Delta p(t), \\ \Delta p(t) &= f\left(\boldsymbol{x}(t)\right), \end{cases} \tag{3.55}$$

where the variables are given by

$$\boldsymbol{w} = \begin{bmatrix} h \\ \dot{h} \end{bmatrix}, \quad \boldsymbol{u} = \begin{bmatrix} h_0 \\ p_m \\ p^- \end{bmatrix}, \quad \boldsymbol{x} = \begin{bmatrix} u_f \\ h \end{bmatrix},$$

where $\boldsymbol{w}$ is the state vector of the reed, $\boldsymbol{u}$ collects the incoming pressure wave p^- and external control parameters such as mouth pressure p_m and the rest opening h_0.

The matrices are

$$\boldsymbol{A} = \begin{bmatrix} 0 & 1 \\ -\omega_0^2 & -g \end{bmatrix}, \quad \boldsymbol{B} = \begin{bmatrix} 0 & 0 & 0 \\ \omega_0^2 & 0 & 0 \end{bmatrix}, \quad \boldsymbol{C} = \begin{bmatrix} 0 \\ -1/\mu \end{bmatrix},$$

$$\boldsymbol{D} = \begin{bmatrix} 0 & -S_r \\ 1 & 0 \end{bmatrix}, \quad \boldsymbol{E} = \begin{bmatrix} 0 & 1/Z_0 & -2/Z_0 \\ 0 & 0 & 0 \end{bmatrix}, \quad \boldsymbol{F} = \begin{bmatrix} -1/Z_0 \\ 0 \end{bmatrix}.$$

The beating condition in Eq. (3.50) is rewritten as

$$\boldsymbol{w} = \boldsymbol{0}, \qquad \text{for} \quad h \leq 0.$$

Note that system (3.55) is formally identical to the general structure (3.43) that we have studied in section 3.4.4. Its first equation can be discretized with one of the techniques described in section 3.4.3. We choose here the bilinear transform, and the discrete-time system is obtained through applications of the transforms *Laplace* $\rightarrow$ *Bilinear* $\rightarrow \mathcal{Z}^{-1}$, where $\mathcal{Z}^{-1}$ is the inverse $\mathcal{Z}$ transform:

$$s \cdot \boldsymbol{W}(s) = \boldsymbol{A}\boldsymbol{W}(s) + \boldsymbol{B}\boldsymbol{U}(s) + \boldsymbol{C}\Delta P(s) \qquad s = h\frac{1-z^{-1}}{1+z^{-1}}, \quad h = 2F_s$$

$$\begin{aligned} \boldsymbol{w}[n] &= [h\boldsymbol{I} - \boldsymbol{A}]^{-1}\{[h\boldsymbol{I} + \boldsymbol{A}]\boldsymbol{w}[n-1] + \boldsymbol{B}[\boldsymbol{u}[n] + \boldsymbol{u}[n-1]] + \boldsymbol{C}[\Delta p[n] + \Delta p[n-1]]\} \\ &= \tilde{\boldsymbol{w}}[n] + \bar{\boldsymbol{C}}\Delta p[n]. \end{aligned} \tag{3.56}$$

Here the vector $\tilde{\boldsymbol{w}}[n]$ is a linear combination of all the terms that are computable at time n (namely $\boldsymbol{u}[n]$ and past values of $\boldsymbol{w}$, $\boldsymbol{u}$ and Δp) while the vector $\bar{\boldsymbol{C}}$ weights the dependence of $\boldsymbol{w}$ on $\Delta p[n]$.

M-3.14

Construct the dynamic reed model according to equation (3.56), as a functions that takes a pressure wave $p^-[n]$ from the bore and returns the computable state vector $\tilde{\boldsymbol{w}}[n]$.

The second equation in system (3.55) can thus be written as

$$\boldsymbol{x}[n] = \tilde{\boldsymbol{x}}[n] + \boldsymbol{K}\Delta p[n], \text{ with } \begin{cases} \boldsymbol{K} &= (\boldsymbol{D}\bar{\boldsymbol{C}} + \boldsymbol{F}) \\ \tilde{\boldsymbol{x}}[n] &= \boldsymbol{E}\boldsymbol{u}[n] + \boldsymbol{D}[h\boldsymbol{I} - \boldsymbol{A}]^{-1}\{(h\boldsymbol{I} + \boldsymbol{A})\boldsymbol{w}[n-1] \\ &\quad + \boldsymbol{B}[\boldsymbol{u}[n] + \boldsymbol{u}[n-1]] + \boldsymbol{C}\Delta p[n-1]\}, \end{cases} \tag{3.57}$$

where $\boldsymbol{K} = (\boldsymbol{D}\bar{\boldsymbol{C}} + \boldsymbol{F})$ weights the delay-free loop connecting Δp to $\boldsymbol{x}$, while the vector $\tilde{\boldsymbol{x}}[n]$ has no instantaneous dependence on $\Delta p[n]$ and is therefore computable at each step. The discrete-time non-linear relation is

$$\Delta p[n] = f\left(\tilde{\boldsymbol{x}}[n] + \boldsymbol{K}\Delta p[n]\right), \tag{3.58}$$

Note that equations (3.56, 3.57, 3.58) are formally identical to the general structure (3.44) that we have studied in section 3.4.4. In particular, equation (3.58) emphasizes the occurrence of a delay-free computational loop in the system, which ultimately causes $\Delta p[n]$ to depend on itself through the non-linear map f. We choose to solve equation (3.58) using Newton iteration: at each time n we look for a zero of the function $g_{\tilde{x}}(\Delta p) = f(\tilde{\boldsymbol{x}} + \boldsymbol{K}\Delta p) - \Delta p$, using the value $\Delta p[n-1]$ as the starting point for the iteration.

M-3.15

Construct the non-linear pressure model according to equation (3.58), as a function that takes the computable input $\tilde{x}$ from the bore and the reed, and returns the pressure drop $\Delta p[n]$.

3.5.4 Properties of the model

3.5.4.1 The numerical reed

We are finally able to analyze the results provided by the discrete-time model developed so far. A first evaluation criterion amounts to examine the reed frequency response. Consider the transfer function $H_r(s)$ in Eq. (3.49) and the corresponding frequency response $H_r(j\omega)$. The transfer function $H_{dr}(z)$ of the digital reed is obtained by substitution:

$$H_{dr}(z) = H_r\left(h\frac{1-z^{-1}}{1+z^{-1}}\right), \tag{3.59}$$

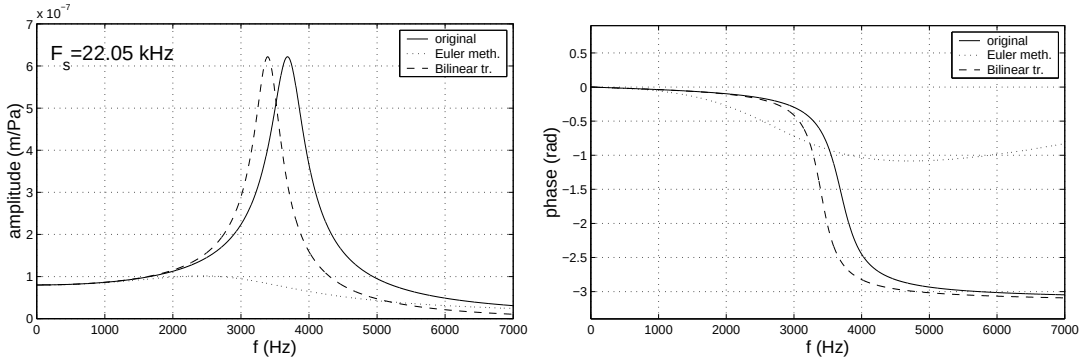

(a) (b)

Figure 3.21: Reed response: comparison of the continuous-time system and the discrete-time systems obtained using the bilinear transform and the Euler method, with $F_s = 22.05$ kHz; (a) magnitude responses and (b) phase responses.

and the corresponding frequency response is given by $H_{dr}\left(\exp(j\omega_d/F_s)\right)$.

Figure 3.21 shows the two responses H_r and H_{dr} in the case $F_s = 22.05$ kHz. The response obtained by applying the Euler method is also plotted as a term of comparison. The Euler method is easily seen to provide poor accuracy. In particular, a noticeable numerical dissipation is introduced, so that the resonance is strongly attenuated. Results for H_{dr} are in good agreement with theoretical predictions. Both the magnitude and the phase responses exhibit frequency warping (see the discussion in Sec. 3.4.3). The original resonance ω_0 has shifted from 23250 rad/s to 21300 rad/s (i.e. from 3700 Hz to 3390 Hz) for H_{dr}.

3.5.4.2 Time-domain simulations

Besides frequency-domain analyis, we can also study the output of the simulations in the time domain by capturing relevant signals ($y_L,\ \Delta p,\ p^{\pm},\ u_f, \ldots$) from each part of the model.

M-3.16

Implement the complete dynamic clarinet model: using the functions developed in M-3.11, M-3.14, and M-3.15, write an audio cycle in which the system is initialized with a certain mouth pressure p_m and evolves freely. Plot the signal and its spectrogram.

Figure 3.22 shows the signal $p(t)$ when a step mouth pressure $p_m = 1900$ Pa is applied. A rich attack transient can be noticed, which is not obtained using simpler models such as the quasi-static one described previously. At steady state the signal resembles the square wave which is typically associated to the clarinet. Note however that even during steady state the quasi-static approximation does not hold: this is shown in figure 3.23, which has been obtained by applying a step mouth pressure $p_m = 2265$ Pa that causes beating to initiate. The figure shows that u_f and Δp move along a hysteretic path, due to the presence of memory in the equations.

Another significant difference between the quasi-static and the dynamic model is concerned with transitions to high regimes of oscillation. Both ω_0 and g play a role in helping transition to the second register (clarion register), which can be produced without opening the register hole if the reed resonance matches a low harmonic of the playing frequency and the damping is small enough.

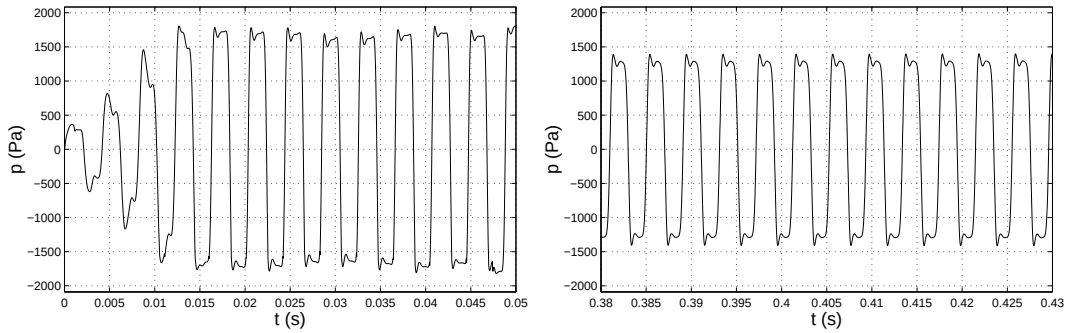

(a) (b)

Figure 3.22: Mouthpiece pressure $p(t)$; (a) attack transient and (b) steady-state signal, with $p_m = 1900$ Pa and $F_s = 22.05$ kHz.

Moreover, an extremely low damping causes the reed regime ("squeaks") to be produced, i.e. the oscillation is governed by the reed resonance. All these effects are seen to be well reproduced by numerical simulations with the digital reed, while on the contrary the quasi-static approximation does not allow control on such effects. Figure 3.24(a) shows an example of transition to the clarion register. This example has been obtained by matching ω_0 to the seventh harmonic of the playing frequency and by lowering g down to 1400 rad/s. Figure 3.24(b) shows a transition to the reed regime. This is achieved by giving g a value as low as 300 rad/s. Squeaks are more easily obtained in simulations by driving the reed with low blowing pressures.

3.6 Key concepts

⇝ Source models vs. signal models

Physical modeling techniques differ drastically from those examined in the previous chapter. Signal-based techniques are derived and characterized by looking at the waveforms produced by the algorithms and their features in the time-domain or in the frequency domain. Source-based techniques try to describe sounds in terms of the physical objects and interactions that are responsible for sound generation.

We have pointed out the implications of this approach in terms of sound representation: a physical model provides a highly semantic description in which the control parameters of the final synthesis algorithms have most of thes a clear physical interpretation (e.g. the length of a string, the stiffness of a reed, and so on), and the algorithms react in a physically consistent way to changes in such parameters.

⇝ Structural aspects: exciters, resonators, non-linearities

In many cases an acoustic system can be represented as composed by resonating structures connected to excitation elements. This distinction is important from the modeling point of view, since the resonating structures (e.g. strings, membranes, bars, plates, acoustic bores, etc.) can be assumed to be linear with good approximation. On the other hand the excitation mechanisms (e.g. impacts, frictions, pressure-controlled valves, air jets, etc.) are typically described by non-linear equations, and determine the way energy is injected into the resonators.

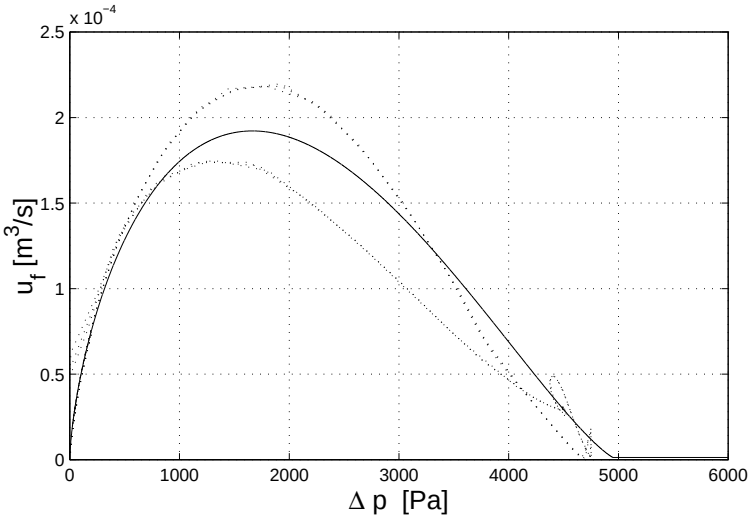

Figure 3.23: Quasi-static curve (solid line) and phase diagram obtained from simulations, with $p_m = 2265$ Pa and $F_s = 22.05$ kHz.

Resonating and exciter blocks are typically connected in a feed-back fashion: as an example, when a bow slides onto a violin string both the objects are subject to an interaction (friction) force which is in turn determined by their relaTive velocity (and possibly other variables). Similar consideration apply to the system composed by a resonating bore and a reed. One case where the coupling can be assumed feed-forward to a goof approximation is that of a plucked string: in ideal pluck simply imposed a non-equilibrium initial displacement to the string, which subsequently oscillates freely.

⇝ Modeling approaches: distributed, lumped

A way of looking at physical modeling techniques is by classifying them into two main categories. Generally speaking, distributed approaches include all the modeling techniques in which the mathematical description takes the spatial distribution of the physical system into account. A description based on a set of partial differential equations (PDEs), simulated through finite difference/elements methods (FDM/FEM), is certainly a distributed modeling approach. Waveguide structures are another example of distributed models: these can in general provide more efficient algorithms with respect to FEM/FDM methods, but are less general.

The category of lumped models includes all of those modeling approaches that do not embed a notion of spatial distribution: describing a piano hammer as an ideal point mass is a lumped modeling approach; similarly, describing a single reed as a second order mechanical oscillator, as we did in section 3.5 and in equation (3.48), is a lumped approach since it does not account for the presence of higher modes of oscillation, for non even pressure distributions on the reed surface, for propagation of vibrations inside the reed.

⇝ The Karplus-Strong (KS) algorithm

We have examined the KS algorithm as a first elementary example of waveguide structure. Its basic building block is a comb filter, whose block scheme and magnitude response are depicted

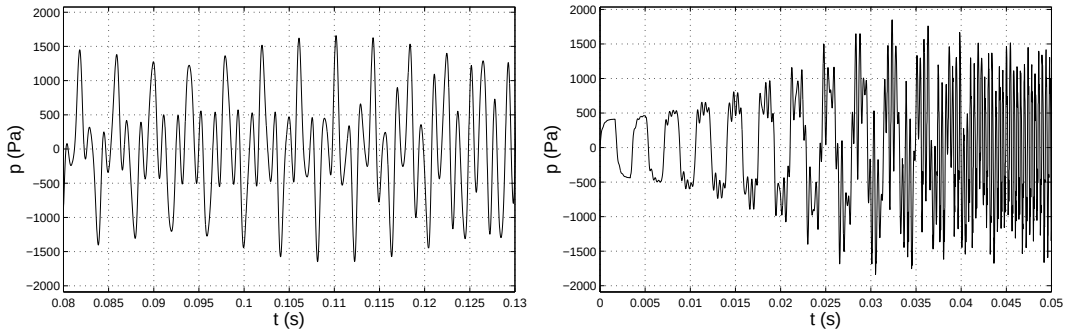

(a) (b)

Figure 3.24: Transitions to high regimes of oscillation; (a) clarion register ($\omega_0 = 2\pi \cdot 2020$ rad/s, $g = 1400$ rad/s, $p_m = 1800$ Pa); (b) reed regime ($\omega_0 = 2\pi \cdot 3150$ rad/s, $g = 300$ rad/s, $p_m = 1900$ Pa).

in figures 3.3(a) and (b), respectively: this show that the comb filter structure is well suited for representing a resonant system with a harmonic spectrum, such as an ideal string with fixed ends. If an additional low-pass filter is inserted into the structure, as in figure 3.5(a), a more realistic response is obtained in which the higher harmonic partials are more damped than the lower ones (see figure 3.5(b)). The original formulation of the KS algorithm assumes that the state of the comb filter is initialized with random values, after which the filter evolves freely: the resulting sounds mimic quite closely those of a guitar string.
The KS filter can be given the following proto-physical interpretation: a displacement wave travels into the string and is reflected back each time it reaches one of the fixed ends. At each reflection the high-frequency components are smoothed away more strongly than the low-frequency ones, because of dissipation phenomena occurring in the string. The theory of 1-D waveguide structures provides a more formal framework to this interpretation.

⇝ 1-D waveguide (WG) structures

We have seen that the starting point in the construction of basic WG structures are the D'Alembert equation and its traveling wave solution. A computational realization of such a solution can be constructed using a pair of delay lines, which simulate wave propagation in the two directions of a 1-D medium. The delay lines are terminated by reflection coefficients that simulate ideal boundary conditions and. Refinements to this basic structures include the modling of dissipation and dispersion, as well as fine tuning elements. All of these are simulated by inserting additional filtering elements into the WG structure: low-pass filters account for frequency-dependent dissipation, while all-pass filters are used to introduce frequency-dependent propagation velocity (an example where dispersion plays a relevant role are piano strings in the low register). Fine tuning is realized through insertion of all-pass linear-phase filters: the phase characteristics of the filter is responsible for an additional fractional delay, which is used to tune the physical length of the modeled resonator (e.g. a string).

⇝ WG networks

Waveguide sections can be connected to each other using juctions that account for impedance

discontinuities in the propagating medium (e.g., two cylindrical bore sections with different diameters, or two pieces of string with different mass densities). When such discontinuities are encountered, scattering occurs, i.e. the incoming waves are partly transmitted and partly reflected. The Kelly-Lochbaum junction is used to connect two waveguide section: its equations (3.19) are derived by imposing continuity conditions for the Kirchoff variables at the junction. We have drawn the block scheme of a KL junction in figure 3.9 and we have seen that a reflection coefficient ρ determines the relative amounts of reflected and transmitted waves. We have also seen that the KL junction can be extended to the n-dimensional case.

⇝ Lumped modeling

We usually look at electrical systems using a lumped approach: current intensity i and voltage v are measured punctually, withouth looking at propagation effects within the circuit. Circuit elements are also described using punctual input-output relations: voltage and current through an element are related via circuit *impedances*, as summarized in Eq. (3.23).

We have seen that mechanical and acoustic systems can be looked at using the same approach. Specifically, we have defined pair of variables (*Kirchoff variables*) that are analogous to voltage and current: these are the pairs force-velocity and pressure-flow, in the case of mechanical and acoustic systems, respectively. For the three classes of systems (electrical, mechanical, acoustic) we have examined the basic impedance blocks and have pointed out the analogies between them. These are summarized in the fundamental Table 3.1. We have also introduced the concepts of parallel and series junctions of mechanical and acoustic elements, and have provided examples in figures 3.12 and 3.13. Finally, we have seen through an example (the Chua-Felderhoff circuit and the non-linear hammer felt) that analogies between classes of systems extend to the case of non-linear elements.

⇝ Modal synthesis

The second-order oscillator (3.29) is the simplest possible resonating mechanical system that we can construct using basic impedances blocks. Simple equations relate the impedances m, r, k to the resonator parameters: center frequency, quality factor, $1/e$ decay time. A set of N oscillators driven by the same force can be used to describe a set of N resonances of a mechanical structure: the mass m of each oscillator determines the amount of the excitation provided by the force to the corresponding resonance.

Up to this point, modal synthesis seems little more than a variant of additive synthesis. However, we have seen that this technique does have a profound physical foundation. Given a set of N point-masses connected through springs and dampers, there exists in general a *modal decomposition* of the system, i.e. a linear transformation that turns the system into a set of decoupled second-order equations. The relation between the mass displacements and the new modal displacements are summarized by Eq. (3.32). Finally, we have observed that by giving the modal masses different values at each of the N points of the physical structure, one can simulate position-dependent interaction (in particular, nodal points correspond to infinite modal masses).

⇝ Discretization methods

WG are already in the discrete-time domain, but in general a physical model is developed in the

continuous-time domain. In particular, lumped modeling approaches describe a system as a set of ordinary differential equations (ODEs). We have briefly examined various approaches to discretization, namely the impulse invariant method and s-to-z techniques such as the (backward) Euler method and the bilinear transform. Each of these approaches carries its own advantages and drawbacks: some of the features that we have analyzed include frequency aliasing and frequency warping, stability, order of accuracy, and numerical damping. We have also defined the concepts of explicit and implicit numerical methods, and looked at the general form of the difference equations that they produce.
Wave digital filters (WDF) can be used to describe a lumped element in the digital domain: first, the impedance of the element is turned into a *reflectance* through a variable transformation, from Kirchoff to wave (as we did in equation (3.39)). Second, the bilinear transform is used to turn such reflectance filters into their digital counterparts. Third, filtering elements are connected by *adapting* their reference impedances in order to avoid the occurrence of delay-free computational loops.

⇝ Computational aspects

The *delay-free loop* problem deserves some discussion, due to the fact that sound physical models typically involve the presence of non-linear elements. We have first examined the problem by looking at a simple example of a linear system, in figure 3.17. In this case the computation can be rearranged into an equivalent structure, but it is clear that such a rearrangement can only be performed under the hypothesis of linearity: when a non-linear element is involved in the computation, we do not know in general whether it is invertible or not.
We have listed some of the approaches that can be taken to deal with the general non-linear case: use of explicit numerical methods, artificial introduction of delay elements in the computation, use of iterative solvers or predictor-corrector combinations. Again, each of these approaches carries its own advantages and drawbacks.

3.7 Commented bibliography

Sound modeling techniques can be classified according to many criteria. Two general references that address these issues are De Poli [1991], Smith III [1991]. Specifically, the taxonomy based on *signal models* and *source models*, and their subclasses, proposed at the beginning of this chapter is based on De Poli [1991].

Seminal ideas that eventually lead to the definition of physically-based sound modeling techniques are to be found in research on musical instrument acoustics. Some classic papers in this area are Hiller and Ruiz [1971a,b], Schumacher [1981], McIntyre et al. [1983]. In particular, the two citations in section 3.2.1 are taken from Hiller and Ruiz [1971a], McIntyre et al. [1983], respectively. A book that covers the topic of musical acoustics exhaustively is Fletcher and Rossing [1991].

A general overview on approaches and techniques used in physical modeling, with an emphasis on structural and computational aspects, is De Poli and Rocchesso [1998]. Figure 3.1 in this chapter (typical block scheme of a musical instrument model) is based on an analogous scheme in De Poli and Rocchesso [1998]. On the other hand, figure 3.2(b) (typical block scheme of an articulatory synthesizer) is based on an analogous scheme in Sondhi and Schroeter [1987].

About distributed modeling approaches: finite difference schemes applied to PDE descriptions have been used in the literature e.g. for modeling idiophones Chaigne and Doutaut [1997] and single

reed systems Stewart and Strong [1980]. The theory of 1-D waveguide models is now well established. An exhaustive introduction to the topic is Smith III [1998], which provides full derivations of waveguide structures and examples of musical instrument modeling, together with a vast bibliography. The Karplus-Strong algorithm, which we have regarded as the first step toward the development of digital waveguide structures, was originally presented in Karplus and Strong [1983].

Many textbooks on digital speech processing contain discussion about multitube lossless models of the vocal tract, which are basically cylindrical waveguide sections connected by Kelly-Lochbaum junctions: see e.g. Deller et al. [1993]. We have not addressed the topic of higher dimensional (2- and 3-D) waveguide structures: seminal ideas were presented in van Duyne and Smith III [1993].

About lumped modeling approaches: a discussion of the analogies between electrical systems and their acoustical counterparts is found in Fletcher and Rossing [1991]. In particular, the circuit representation of a Helmoltz resonator given in section 3.4.1 is based on an analogous discussion in Fletcher and Rossing [1991]. A classic presentation of modal synthesis techniques is Adrien [1991]. We have examined in section 3.5 an example of lumped element physical model (the single reed): this model has been used extensively in the literature, see e.g. Schumacher [1981]. A classic example of a lumped physical model applied to voice synthesis is Ishizaka and Flanagan [1972], in which the authors describe the vocal folds by means of two lumped masses and viscoelastic elements.

About numerical and computational aspects: most of the techniques described in section 3.4.3 are found in DSP textbooks: see e.g. Mitra [1998]. A classic reference to the theory of Wave Digital Filters (*WDF*) theory is Fettweis [1986]. In the field of numerical analysis, a comprehensive discussion on numerical methods for ordinary differential equations is given in Lambert [1993]. The example that we discussed in section 3.4.4 about delay-free computational paths in linear systems (see figure 3.17) is adapted from [Mitra, 1998, section 6.1.3, Fig. 6.5]. We have seen that new problems are encountered when non-linear elements are present in the delay-free computational path: reference Borin et al. [2000] provides a discussion of these issues, together with a proposed non-iterative solution (in brief, a set of hypotheses and techniques to compute *a priori* the non-linear function $\boldsymbol{h}$ that we have examined in section 3.4.4), and applications to the simulation of acoustic systems. We have followed the notation given in Borin et al. [2000] for the matrices in equation (3.43) and for the $\boldsymbol{K}$ matrix in equation (3.44).

References

J. M. Adrien. The Missing Link: Modal Synthesis. In G. De Poli, A. Piccialli, and C. Roads, editors, *Representations of Musical Signals*, pages 269–297. MIT Press, 1991.

G. Borin, G. De Poli, and D. Rocchesso. Elimination of Delay-free Loops in Discrete-Time Models of Nonlinear Acoustic Systems. *IEEE Trans. Speech Audio Process.*, 8(5):597–606, Sep. 2000.

A. Chaigne and V. Doutaut. Numerical Simulations of Xylophones. I. Time-domain Modeling of the Vibrating Bar. *J. Acoust. Soc. Am.*, 101(1):539–557, Jan. 1997.

G. De Poli. A Tutorial on Digital Sound Synthesis Techniques. In C. Roads, editor, *The Music Machine*, pages 429–447. MIT Press, 1991.

G. De Poli and D. Rocchesso. Physically Based Sound Modelling. *Organized Sound*, 3(1):61–76, 1998.

J. R. Deller, J. G. Proakis, and J. H. L. Hansen. *Discrete-Time Processing of Speech Signals*. Macmillan, New York, 1993.

A. Fettweis. Wave Digital Filters: Theory and Practice. *Proc. IEEE*, 74(2):270–327, Feb. 1986.

N. H. Fletcher and T. D. Rossing. *The Physics of Musical Instruments*. Springer-Verlag, New York, 1991.

L. Hiller and P. Ruiz. Synthesizing Musical Sounds by Solving the Wave Equation for Vibrating Objects: Part I. *J. Audio Engin. Soc.*, 19(6):462–470, June 1971a.

L. Hiller and P. Ruiz. Synthesizing Musical Sounds by Solving the Wave Equation for Vibrating Objects: Part II. *J. Audio Engin. Soc.*, 19(7):542–551, July 1971b.

K. Ishizaka and J. L. Flanagan. Synthesis of Voiced Sounds from a Two-Mass Model of the Vocal Cords. *Bell Syst. Tech. J.*, 51:1233–1268, 1972.

K. Karplus and A. Strong. Digital Synthesis of Plucked String and Drum Timbres. *Computer Music J.*, 7(2):43–55, 1983.

J. D. Lambert. *Numerical Methods for Ordinary Differential Systems*. John Wiley & Sons, 1993.

M. E. McIntyre, R. T. Schumacher, and J. Woodhouse. On the Oscillations of Musical Instruments. *J. Acoust. Soc. Am.*, 74 (5):1325–1345, Nov. 1983.

S. K. Mitra. *Digital Signal Processing. A Computer Based Approach*. Mc Graw Hill, 1998.

R. T. Schumacher. *Ab Initio* Calculations of the Oscillations of a Clarinet. *Acustica*, 48(2):71–85, 1981.

J. O. Smith III. Viewpoints on the History of Digital Synthesis. In *Proc. Int. Computer Music Conf. (ICMC'91)*, pages 1–10, Montreal, Oct. 1991.

J. O. Smith III. Principles of Digital Waveguide Models of Musical Instruments. In M. Kahrs and K. Brandenburg, editors, *Applications of DSP to Audio and Acoustics*, pages 417–466. Kluwer Academic Publishers, 1998.

M. M. Sondhi and J. Schroeter. A Hybrid Time-Frequency Domain Articulatory Speech Synthesizer. *IEEE Trans. Acoust., Speech, and Sig. Process.*, 35(7):955–967, July 1987.

S. E. Stewart and W. J Strong. Functional Model of a Simplified Clarinet. *J. Acoust. Soc. Am.*, 68(1):109–120, July 1980.

S. A. van Duyne and J. O. Smith III. The 2-D Digital Waveguide Mesh. In *Proc. IEEE Workshop on Applications of Sig. Process. to Audio and Acoustics (WASPAA'93)*, pages 177–180, New Paltz (NY), Oct. 1993.

Contents

3 Sound modeling: source-based approaches **3.1**

3.1 Introduction: sounds, sources . . . 3.1
3.2 Structures, functions, models . . . 3.2
3.2.1 Functional blocks . . . 3.2
3.2.1.1 Excitations and resonators . . . 3.2
3.2.1.2 Analogies with speech synthesis . . . 3.3
3.2.2 Modeling approaches . . . 3.5
3.3 Distributed models: the waveguide approach . . . 3.6
3.3.1 The origins: the Karplus-Strong algorithm . . . 3.6
3.3.1.1 The comb filter . . . 3.6
3.3.1.2 Refining the structure . . . 3.7
3.3.2 One-dimensional wave propagation . . . 3.9
3.3.2.1 Traveling wave solution . . . 3.9
3.3.2.2 One-dimensional propagation . . . 3.10
3.3.2.3 Wave variables . . . 3.11
3.3.3 Basic waveguide structures . . . 3.12
3.3.3.1 Delay lines . . . 3.12
3.3.3.2 Boundary conditions . . . 3.12
3.3.4 Modeling real world phenomena . . . 3.13
3.3.4.1 Dissipation . . . 3.13
3.3.4.2 Dispersion . . . 3.14
3.3.4.3 Length tuning . . . 3.15
3.3.5 Junctions and networks . . . 3.16
3.3.5.1 The Kelly-Lochbaum junction . . . 3.16
3.3.5.2 N-dimensional junctions . . . 3.17
3.3.5.3 Non-cylindrical geometries . . . 3.18
3.4 Lumped models . . . 3.19
3.4.1 Building blocks and analogies . . . 3.19
3.4.1.1 Mechanical systems . . . 3.19
3.4.1.2 Acoustic systems . . . 3.21
3.4.1.3 Non-linearities . . . 3.22
3.4.2 Modal synthesis . . . 3.24
3.4.2.1 The second-order mechanical oscillator . . . 3.24
3.4.2.2 The modal description . . . 3.24
3.4.3 Numerical methods . . . 3.26
3.4.3.1 Impulse invariant method . . . 3.26

3.4.3.2 Mappings "s-to-z" . . . 3.26
3.4.3.3 Accuracy, stability . . . 3.27
3.4.3.4 Wave digital filters . . . 3.29
3.4.4 Computability issues . . . 3.29
3.4.4.1 The delay-free loop problem . . . 3.30
3.4.4.2 Approaches . . . 3.31
3.5 A full example: the clarinet . . . 3.33
3.5.1 Functional blocks . . . 3.34
3.5.1.1 Resonator: the bore . . . 3.34
3.5.1.2 Excitation: the reed . . . 3.34
3.5.2 The quasi-static approximation . . . 3.36
3.5.3 The dynamic reed model . . . 3.37
3.5.4 Properties of the model . . . 3.38
3.5.4.1 The numerical reed . . . 3.38
3.5.4.2 Time-domain simulations . . . 3.39
3.6 Key concepts . . . 3.40
3.7 Commented bibliography . . . 3.44